

Extracting trap depth distributions in persistent phosphors with a thermal barrier for charging

Ang Feng,^{1,2} Jiaren Du,^{1,2} and Philippe F. Smet^{1,2,*}

¹*Lumilab, Department of Solid State Sciences, Faculty of Sciences,
Ghent University, Krijgslaan 281-S1, Ghent 9000, Belgium*

²*Center for Nano- and Biophotonics (NB-Photonics), Ghent University, Belgium*

(Dated: June 3, 2022)

The trap depth distribution in persistent phosphors, along with the charging and working conditions, determines the performance of these phosphors. Extracting the trap depth distribution is often hindered by the presence of a thermal barrier for charging, which leads to temperature-dependent filling of traps. Within the framework of a local charge transition for the trapping and recombination, we propose a method for extracting the trap depth distribution from electron population functions. They were converted from thermoluminescence curves via the Tikhonov regularization in the framework of first-order kinetics. The theoretical model predicts the evolution of a filling function for the traps with increasing charging temperature. The relative filling functions at different charging temperature, together with the corresponding electron population function, were used to reconstruct the actual underlying trap depth distribution. The method provides good precision and resolution. Trap depth distributions deepen our understanding of the properties of persistent phosphors.

I. INTRODUCTION

It is a materials scientist's dream to tailor materials properties by tuning only a few intrinsic parameters of the materials. This is true for persistent phosphors whose luminescence persist from seconds to days after stopping optical excitation [1–3]. High persistent luminescence (PersL) intensity and long PersL duration are two desirable properties under given optical charging condition and working condition [4]. One critical parameter controlling these properties is the density of traps, i.e., the absolute number of active traps per unit volume of the given persistent phosphor. The higher the trap density, the more charges a phosphor can store at the given charging temperature, enhancing PersL intensity. Another parameter is the distribution of trap density with respect to trap depth E_t , which quantifies the energy barrier trapped electrons must overcome to meet luminescent centers. It is usually called trap depth distribution for short. These parameters are heavily desired for their great scientific importance. At one hand, they are useful to understand and thus to tailor performances of persistent phosphors under different charging and working conditions. For example, the trap depth distribution can be translated into the thermoluminescence (TL) profile, which has been found in a linear relationship to integrated PersL intensity as a function of charging and working temperature [5, 6]. This suggests a subtle relationship between trap depth distribution and the optimum working temperature of persistent phosphors. On the other hand, such parameters act as intrinsic materials parameters that can be compared across different phosphors, enabling the discovery of empirical laws in persistent phosphors. This is particularly true for materials discovery via machine learning [7], where intrinsic materials parameters add reliable dimensions to the parameter space.

There are multiple difficulties when it comes to extracting trap density and trap depth distribution. After optical charging, the density of trapped electrons (called here the electron population function) $n(E_t, t, q)$ is determined by the total trap density N_0 , the trap depth distribution $N(E_t)$ and the filling function $f(E_t, t, q)$ via,

$$n(E_t, t, q) = N_0 f(E_t, \Delta E, t, q) N(E_t), \quad (1)$$

where the charging condition q includes the irradiance $I_e(\lambda)$, the charging duration t_{ch} and the charging temperature T_{ch} . The thermal barrier for charging is ΔE . For the trap depth range $[E_t, E_t + dE]$, $f(E_t, t, q)dE$ is the ratio of the number of filled traps to the total number of traps at time t and at a charging condition of q . The filling function contains the information of how the density of filled traps evolves with time. The trap density accessible at temperature T_{ch} can be approximated by the storage capacity which is actually $n(E_t, t, q)$ in the limit of $t_{ch} \rightarrow \infty, I_e(\lambda) \rightarrow \infty$ [8]. However, the value of storage capacity is expected to be about 1~2 order-of-magnitude smaller than N_0 due to detrapping routes, such as thermal detrapping and optically stimulated detrapping [8–10]. It fails to count shallow

* philippe.smet@UGent.be

traps that are empty at the given charging temperature. Furthermore, a thermal barrier for charging ΔE brings complexity. The maximum of the filling function $f(E_t, t, q)$ depends on charging temperature when there exists a thermal barrier for the charge transfer from the luminescent center to the trap. The presence of such a thermal barrier has been observed in many persistent phosphors, for example $\text{SrAl}_2\text{O}_4:\text{Eu}^{2+}$ [11], $\text{Sr}_2\text{MgSi}_2\text{O}_7:\text{Eu}^{2+}$ [9], and $\text{M}_2\text{Si}_5\text{N}_8:\text{Eu}$ ($\text{M} = \text{Ca}, \text{Sr}, \text{Ba}$) [12]. It hinders the extraction of the trap density or trap depth distribution. Here, we attach more importance to trap distribution $N(E_t)$ than to the total trap density N_0 , because the latter can be inferred from the former along with a storage capacity measurement [8] through some calibration.

Extracting full trap depth distribution has remained largely unresolved because of its complexity, especially in the presence of a thermal barrier for charging. Many methods are already available to extract discrete trap depths [13, 14]. Independent of the order of kinetics, the initial rise method provides a single trap depth from the slope of the logarithm of TL intensity $\ln(I)$ as a function of the inverse of temperature $1/T$ [15, 16]. Combined with a fractional heating and cooling protocol, it has been used to find the electron population function $n(E_t, t, q)$, being given the name of fractional glow technique [17, 18]. The T_m - T_{stop} method utilizes the temperature of TL maximum, T_m , as a function of a preheating temperature T_{stop} [19]. It can estimate the electron population function when used with the Urbach relation [20] or the initial rise method. However, it underestimates the trap depth and fails to extract distributions that overlap [16]. In the case without a charging barrier, K. Van den Eeckhout et al. managed to find the trap depth distribution by acquiring TL profiles from sufficient charging at different charging temperature [21]. Based on the first-order kinetics, $n(E_t, t, q)$ is related to the corresponding TL curve via the Fredholm integral of the first kind, and can be calculated by the Tikhonov regularization method [22]. Furthermore, the thermal barrier ΔE is interesting on its own right, for example in the understanding of the thermal quenching of $\text{Eu}^{2+}/\text{Ce}^{3+}$ emitters [23]. M. Nikl et al. proposed a method to evaluate this quantity, given a trap depth estimated from TL data [24].

The electron population function fails to approximate the trap depth distribution when a thermal barrier of charging ΔE is present. In this work, we propose a method that erases the influence of ΔE and manages to extract the trap depth distribution. The phosphor $\text{BaSi}_2\text{O}_2\text{N}_2:2\%\text{Eu}^{2+}$ was used as a model to validate the proposed method. In addition to novel properties such as PersL [25] and mechanoluminescence [26–28], this phosphor shares high quantum efficiency of photoluminescence and great thermal stability [29], enabling high TL signal strength. Based on the first-order kinetics of charge trapping and recombination, we extract the electron population function $n(E_t)$ via the Tikhonov regularization method. We adopt the following procedure to extract the trap depth distribution.

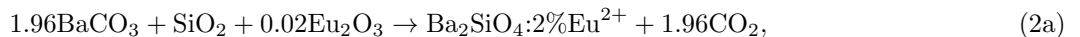
1. Excite the phosphor optically for a duration of t_{ch} at temperature T_{ch} , and cool it down to $T_0 \leq T_{ch} - 30$ K. Then, collect the TL curve with heating rate β . Repeat this step for different T_{ch} , ranging from T_{min} to T_{max} at a step of ΔT (< 10 K). Each TL curve must be corrected by the thermal quenching (TQ) profile.
2. Reconstruct $n(E_t, T_{ch})$ from the TL curves, and calculate the relative filling function $f(E_t, T_{ch}) = \frac{n(E_t, T_{ch})}{n(E_t, T_{min})}$. Estimate the magnitude $f_0(T_{ch})$ from the $f(E_t, T_{ch})$.
3. Construct the envelope $n(E_t)_{env}$ of all $n(E_t, T_{ch})$.
4. Calculate the trap depth distribution according to $N(E_t) = n(E_t)_{env}/f_0(T_{ch})$.

The charging duration t_{ch} should be large enough so that the shape of $n(E_t)$ does not change by further increasing t_{ch} . Cooling from T_{ch} to T_0 not only freezes electrons trapped at shallow traps but also decreases uncertainties of the electron population $n(E_t, T_{ch})$. T_{min} should be low enough such that the shape of TL curves does not change further with decreasing T_{ch} .

Retrapping among traps with different trap depth is one of the processes that leads to global non-first-order transition in the model. However, our experiment confirmed that it is not important when the electron population function is read by TL, consolidating the validity of first-order kinetics. The method is extendable to other materials when the trap depth distribution can be translated into TL. With the trap depth distribution at hand, we are now able to understand the properties of persistent phosphors to the next level and expect interesting applications.

II. MATERIALS AND METHODS

The $\text{BaSi}_2\text{O}_2\text{N}_2:2\%\text{Eu}^{2+}$ phosphor was prepared by a two-stage solid-state reaction method [30], according to:



The raw materials BaCO_3 (99.8 %, 1 μm powder, Alfa Aesar), SiO_2 (99.5%, 325 mesh powder, Alfa Aesar), and Eu_2O_3 (99.9 %, Alfa Aesar) were used in stoichiometric amount except that 103% Si_3N_4 (α phase, 99.9 %, 1 μm

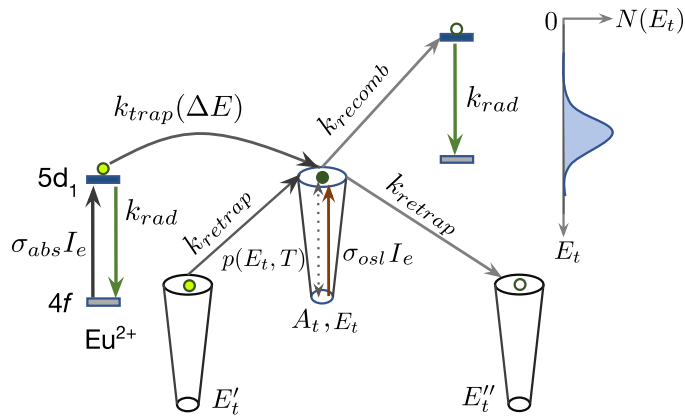


FIG. 1. **The local transition model of persistent phosphors.** During charging, an electron from a luminescent center jumps to its nearby empty traps after overcoming a thermal barrier ΔE , leaving a hole around this ionized luminescent center. Recombination takes place within this electron-hole pair. Retrapping among traps with different trap depth (illustrated as E_t, E'_t, E''_t) is not considered in the present work. The trap depth distribution is $N(E_t)$. k , $p(E_t, T)$ and $\sigma_{osl} I_e$ are rate coefficients.

powder, Alfa Aesar) was supplied to facilitate the reduction of Eu^{3+} to Eu^{2+} [31]. The sintering temperature and duration for Eqn. 2a and Eqn. 2b were 1200 °C, 4 h and 1450 °C, 10 h, respectively. A 94% N_2 -6% H_2 forming gas was applied at a constant rate (0.16 L/min) during the entire thermal process. The product was crushed and ground to fine powders, and then washed by diluted hydrogen chloride (HCl , <1 vol%). After being dried at 80 °C for at least 10 h, $\text{BaSi}_2\text{O}_2\text{N}_2:2\%\text{Eu}^{2+}$ powders were finally ready.

A thermal quenching (TQ) profile was collected to correct TL curves by using the method proposed in Ref [32]. The spectra were acquired at a home-built setup which is capable of providing wavelength resolution at both excitation and detection sides [11]. The excitation light of 370 nm (full-width-half-maximum (fwhm) 5 nm) was from a Xe arc lamp equipped with a monochromator, while the emission was collected by an EMCCD camera (Princeton Instruments ProEM 1600) coupled to a spectrograph (Princeton Instruments Acton SP2300). The integration time was 1 s. The phosphor was cooled to 213 K and then heated to 498 K at a step of 5 K, with optical excitation at each temperature T for 30 s. For each T , five spectra from the time range from 24 to 28 s were averaged to represent the PL emission intensity $I(T)$ (Supplemental material (SM) [33], section I).

To acquire a TL curve, the phosphor was first excited at T_{ch} by an LED of 375 nm (fwhm 20 nm, 50 mA) for 300 s, and then cooled down at a rate of 0.5 K/s to T_0 , where the TL intensity is negligible. Finally, the phosphor was heated up to 493 K at a rate of 0.5 K/s. The emission was detected by a photometer (International Light Technologies, ILT1700) equipped with a photopic filter (YPM). Every TL curve was corrected by a modified TQ profile which was the linear interpolation of the measured TQ profile at each temperature recording of the TL curve.

III. THEORY

A. Local transition

There are three main species involved in PersL, namely charge traps, holes, and luminescent centers. A luminescent center, e.g. Eu^{2+} , requires one of its excited states being occupied by an electron in order to shine via radiative transitions. An empty electron trap captures an electron while the filled one supplies an electron to recombine with a hole nearby. Traps can be lattice defects [34] or co-dopants [35]. A hole consists of an ionized luminescent center. Upon receiving an electron from a filled trap, it can turn itself into a luminescent center at its excited states, whose de-excitation yields light. In parallel, a hole can act as the charge carriers and thus may be trapped in hole traps [36]. The fact that trapped electrons escape from traps via thermal energy suggests the presence of excited states of traps.

Local transitions among luminescent centers, traps and holes provide first-order kinetics and reasonable interpretation of the trapping process. The illustration of trapping and recombination processes is shown in Fig. 1. Upon optical charging, the excited state of a luminescent center (e.g. Eu^{2+}) will be occupied via an internal electronic transition of an electron from the ground state. In addition to subsequent spontaneous emission, this excited electron can jump to an empty trap nearby after crossing a thermal barrier ΔE . This process is termed trapping, which takes

place within the electron-trap pair composed of an electron at the excited state of a luminescent center and a nearby empty trap. This transition leaves a hole at the luminescent center. When it receives an electron from the excited state of a filled trap, it can turn itself into an excited luminescent center, producing light upon de-excitation. This is the recombination process. It takes place within the electron-hole pair composed of an electron at the excited state of a filled trap and a hole nearby. It is noteworthy that an electron-trap pair comes into existence from a center-trap pair composed of an active luminescent center and an empty trap. The electron transfer from a filled trap to another empty trap, i.e. retrapping, is not considered here.

Assuming first-order kinetics in the local transition model is very reasonable for persistent phosphors working under laboratory conditions. The reasons are two-fold. At one hand, the concentration of the luminescent centers (usually at the order of 1 mol%) is often greater than that of the empty traps when they are lattice defects. In this case, electron-trap pairs are far from each other and are thus well isolated because the density of electron-trap pair is far less than that of center-center pair. On the other hand, empty traps can often only be filled to a limited level via exciting the luminescent centers, even if the density of traps is high, as is the case of Dy in $\text{Sr}_4\text{Al}_{14}\text{O}_{25}:\text{Eu}^{2+}, \text{Dy}^{3+}$ [35]. This originates from small optical absorption cross-sections of luminescent centers and additional detrapping routes that empty filled traps, such as optically stimulated detrapping [9, 10]. Therefore, an isolated electron-trap pair can only transform into an electron-hole pair thanks to a very limited interaction with other pairs. Hence, the kinetics of the density of these pairs is readily available within the framework of first-order kinetics. In terms of counting pairs, the most prominent pair is the nearest neighbor (NN) pair where one component is the nearest neighbor of its counterpart. The NN assumption translates the density of electron-trap pairs into the density of filled traps. Therefore, the filling function $f(E_t, \Delta E, t)$ follows the first-order ordinary differential equation,

$$\frac{\partial f(E_t, \Delta E, t)}{\partial t} = -k_{recomb}(E_t, I_e)f(E_t, \Delta E, t) + k_{trap}(\Delta E, I_e)[1 - f(E_t, \Delta E, t)], \quad (3)$$

where $k_{trap}(\Delta E, I_e)$ and $k_{recomb}(E_t, I_e)$ are the trapping coefficient and recombination coefficient, respectively.

The quasi-equilibrium approximation (QEA) helps to approximate the transition coefficients. The life time of the excited states of traps and luminescent centers are much shorter than the time scale of interest in PersL or TL experiments. Thus, upon any abrupt δ -function-like perturbation, these excited states reach a quasi-equilibrium in the time scale of observation. After applying QEA to luminescent centers and traps, the trapping coefficient and the recombination coefficients are,

$$k_{trap}(\Delta E, I_e) = \nu_t \exp\left(-\frac{\Delta E}{k_B T}\right) \frac{\sigma_{abs} I_e}{k_{rad}}, \quad (4)$$

$$k_{recomb}(E_t, I_e) = \nu_r \exp\left(-\frac{E_t}{k_B T}\right) + \frac{\nu_r}{A_t} \sigma_{osl} I_e, \quad (5)$$

respectively. Here σ_{abs} is the optical absorption cross section of Eu^{2+} , and k_{rad} is the spontaneous emission coefficient of the lowest 5d state of Eu^{2+} . In parallel for traps, σ_{osl} is the absorption cross section of optically stimulated detrapping, while A_t is the de-excitation coefficient of the excited states regardless of trap depths. The frequency factors ν_r and ν_t are for the trapping of electrons to traps and the recombination of trapped electrons with holes, respectively. After charging, the second term of k_{recomb} , which is due to optically stimulated detrapping, reduces to zero accordingly.

For a phosphor with all traps initially empty, i.e. $f(E_t, \Delta E, I_e, 0) = 0$, an optical charging with fixed irradiance I_e , duration t_{ch} and temperature T_{ch} leads to the filling function as a solution of Eqn. 3,

$$f(E_t, \Delta E, I_e, t_{ch}) = \frac{k_{trap}(\Delta E, I_e)}{k_{trap}(\Delta E, I_e) + k_{recomb}(E_t, I_e)} \{1 - \exp[-(k_{trap}(\Delta E, I_e) + k_{recomb}(E_t, I_e)) t_{ch}]\}. \quad (6)$$

Clearly, the magnitude and shape of the filling function are influenced by the thermal barrier ΔE . It is unrealistic to fit this model to experimental observations directly because the number of parameters are huge and many of them are not easily available. Instead, the behavior of this filling function under controlled condition will be analyzed to extract the trap depth distribution according to Eqn. 1.

B. First order kinetics

First-order kinetics comes naturally when the recombination within the isolated electron-hole pair is considered only, neglecting thus many-body effects, such as retrapping among traps of different trap depth and recombination in

ordered electron-hole clusters. In the framework of first-order kinetics, the TL intensity from an electron population function $n(E_t)$ is,

$$I(T, \beta) = C \times \int_0^\infty n(E_t) \frac{\nu_r}{\beta} \exp\left(-\frac{E_t}{k_B T}\right) \exp\left[-\frac{\nu_r}{\beta} \int_{T_0}^T \exp\left(-\frac{E_t}{k_B T'}\right) dT'\right] dE_t, \quad (7)$$

where β is the heating rate (K/s), and C a scalar. Here, the electron population function $n(E_t)$ takes its value just at the start of heating, where the temperature is T_0 . This is in accordance with the formula proposed by Randall and Willkins [37, 38], who replaced the electron population function $n(E_t)$ in Eqn. 7 with a trap depth distribution $N(E_t)$. As long as T_0 is substantially smaller than T , e.g. 20~30 K will suffice, it can be replaced by 0 K, leading to the temperature integral [39],

$$F(E_t, T) = \frac{\nu_r}{\beta} \int_0^T \exp\left(-\frac{E_t}{k_B T'}\right) dT'. \quad (8)$$

Among many approximations [40], the formula proposed by M. Balarin [41] gives very high accuracy ,

$$F(E_t, T) = \frac{\nu_r k_B T^2}{\beta E_t} \exp\left(-\frac{E_t}{k_B T}\right) \frac{1}{\sqrt{1 + 4k_B T/E_t}}, \quad (9)$$

even when $\frac{E_t}{k_B T}$ is small.

The exponential function in Eqn. 9 suggests that the exponential of temperature integral in Eqn. 7 has its value distributed in narrow range of E_t , where $n(E_t)$ can be reckoned as a constant approximately. We take the derivative,

$$\frac{\partial}{\partial E_t} \ln \left\{ \frac{\nu_r}{\beta} \exp\left(-\frac{E_t}{k_B T}\right) \exp[-F(E_t, T)] \right\} = -\frac{1}{k_B T} + \frac{\nu_r}{\beta} \int_0^T \frac{1}{k_B T'} \exp\left(-\frac{E_t}{k_B T'}\right) dT'$$

to zero and find the solution,

$$E_s = k_B T W(\nu_r T/\beta), \quad (10)$$

in which $W(x)$ is the Lambert W function of x with the branch $n = 0$. After some algebra, we have the Gumbel probe for TL,

$$P(E_t, E_s, \beta) = I_s(E_t, \beta) \exp\left[1 - \frac{E_t - E_s}{k_B T} - \exp\left(-\frac{E_t - E_s}{k_B T}\right)\right], \quad (11)$$

$$I_s(E_t, \beta) = \frac{4k_B}{E_t} W\left(\sqrt{\frac{E_t \nu_r}{4k_B \beta}}\right)^2 \exp\left[-1/\sqrt{1 + 4/W\left(\sqrt{\frac{E_t \nu_r}{4k_B \beta}}\right)}\right], \quad (12)$$

where $I_s(E_t, \beta)$ has an alternative form as a function of temperature T ,

$$I_s(T, \beta) = \frac{W(\nu_r T/\beta)}{T} \exp\left[-1/\sqrt{1 + 4/W(\nu_r T/\beta)}\right].$$

Thus, Eqn. 7 can be rewritten in the following form,

$$I(E_s, \beta) = C \times \int_0^\infty n(E_t) P(E_t, E_s) dE_t. \quad (13)$$

First-order kinetics provides a very lucid physics picture of TL. As the phosphor is heated up at a rate of β , the Gumbel probe (11) scans the electron population $n(E_t)$ from shallow traps to deep traps with the approximate speed of $\beta k_B W(\nu_r T/\beta)$. Its width broadens according to the shape factor $k_B T$, while its magnitude decreases roughly as $W(\nu_r T/\beta)/T$, which is much slower than the algebraic decay of $1/T$.

A special case of TL is the isothermal stimulation in PersL. After charging at T_{ch} , the temperature of the phosphor still stays constant while the luminescence intensity is recorded as a function of delay time t_0 . This is the decay profile for the PersL. The thermal detrapping process in PersL can be described by Eqn. 13 with the Gumbel probe as well,

$$P(E_t, E_s) = \nu_r \exp\left(-\frac{E_t}{k_B T}\right) \exp\left[-\frac{E_t - E_s}{k_B T} - \exp\left(-\frac{E_t - E_s}{k_B T}\right)\right], \quad (14)$$

where $E_s = k_B T \ln(\nu_r t_0)$. As the delay time t_0 increases, the Gumbel probe scans the electron population function from shallow to deep traps at a speed of $k_B T/t_0$. The magnitude of the probe follows the algebraic decay of $1/t_0$. This clearly indicates the presence of the power law of $t_0^{-\beta}$ ($\beta \approx 1$) of the decay profile. It is difficult to infer $n(E_t)$ from the decay profile. The reasons are obvious. It requires a huge range of delay time t_0 to access a reasonably wide range of trap depths. Moreover, the electron population function of deep traps can not be reconstructed faithfully because the magnitude of the Gumbel probe (Eqn. 14) buries the light output in measurement noises.

C. Regularization

Once the physics is clear, we are ready to calculate and interpret the electron population function. This can be done via solving Eqn. 13 after some regularization methods. A better way would be to utilize Eqn. 7 with the temperature integral (Eqn. 9), i.e.,

$$I(T, \beta) = C \times \int_0^\infty n(E_t) K(E_t, T) dE_t, \quad (15)$$

$$K(E_t, T) = \frac{\nu_r}{\beta} \exp\left[-\frac{E_t}{k_B T} - \frac{\nu_r}{\beta} \exp\left(-\frac{E_t}{k_B T}\right) \frac{1}{\sqrt{1 + 4k_B T/E_t}}\right]. \quad (16)$$

The electron population function $n(E_t)$ can be extracted from experimental TL curves via discrete inverse problem technique. Eqn. 15 is a Fredholm integral of the first kind and boils down to a linear equation after discretization over $[T_0, T_m] \times [E_a, E_b]$,

$$Kn = i, \quad (17)$$

where K is the kernel, i the experimental TL data in temperature range $[T_0, T_m]$ and n the electron population function in $[E_a, E_b]$. However, no reliable n can be extracted from Eqn. 17 by linear least square methods, i.e., seeking \hat{n} that minimizes the residual norm squared $\|K\hat{n} - i\|_2^2$. The failure originates from the noise in i and the large condition number of the kernel K . The Tikhonov regularization method minimizes $\|K\hat{n} - i\|_2^2 + \lambda^2 \|L\hat{n}\|_2^2$ instead [42, 43]. Here λ is the regularization parameter, and L is the discrete approximation of a derivative operator. This is equivalent to a modified least square problem,

$$\begin{bmatrix} K \\ \lambda L \end{bmatrix} n = \begin{bmatrix} i \\ 0 \end{bmatrix}. \quad (18)$$

Eqn. 18 can be solved numerically via generalized singular value decomposition (GSVD) given the values of L and λ [43]. The matrix L was chosen to be the discrete analog of the second derivative. We adopt reflexive boundary conditions to avoid possible artifacts of $n(E_t)$ near E_a or E_b . This boundary condition changes the kernel K and matrix L due to the requirement of symmetry. The optimum regularization parameter λ_{opt} can be obtained by the L-curve method [43, 44]. In the supplemental material (SM [33], section II), we provide the implementation of the Tikhonov regularization method by the *Regularization Tools* MATLAB package [45, 46].

IV. RESULTS

A. The filling function

The filling function Eqn. 6 gives the percentage of the filled traps after an optical charging at T_{ch} for a duration of t_{ch} . As shown in Fig. 2a, it reaches a high value for deep traps that are charged at a sufficiently high charging temperature T_{ch} . The parameters in the simulation are estimated from BaSi₂O₂N₂:2%Eu²⁺ or empirical estimations

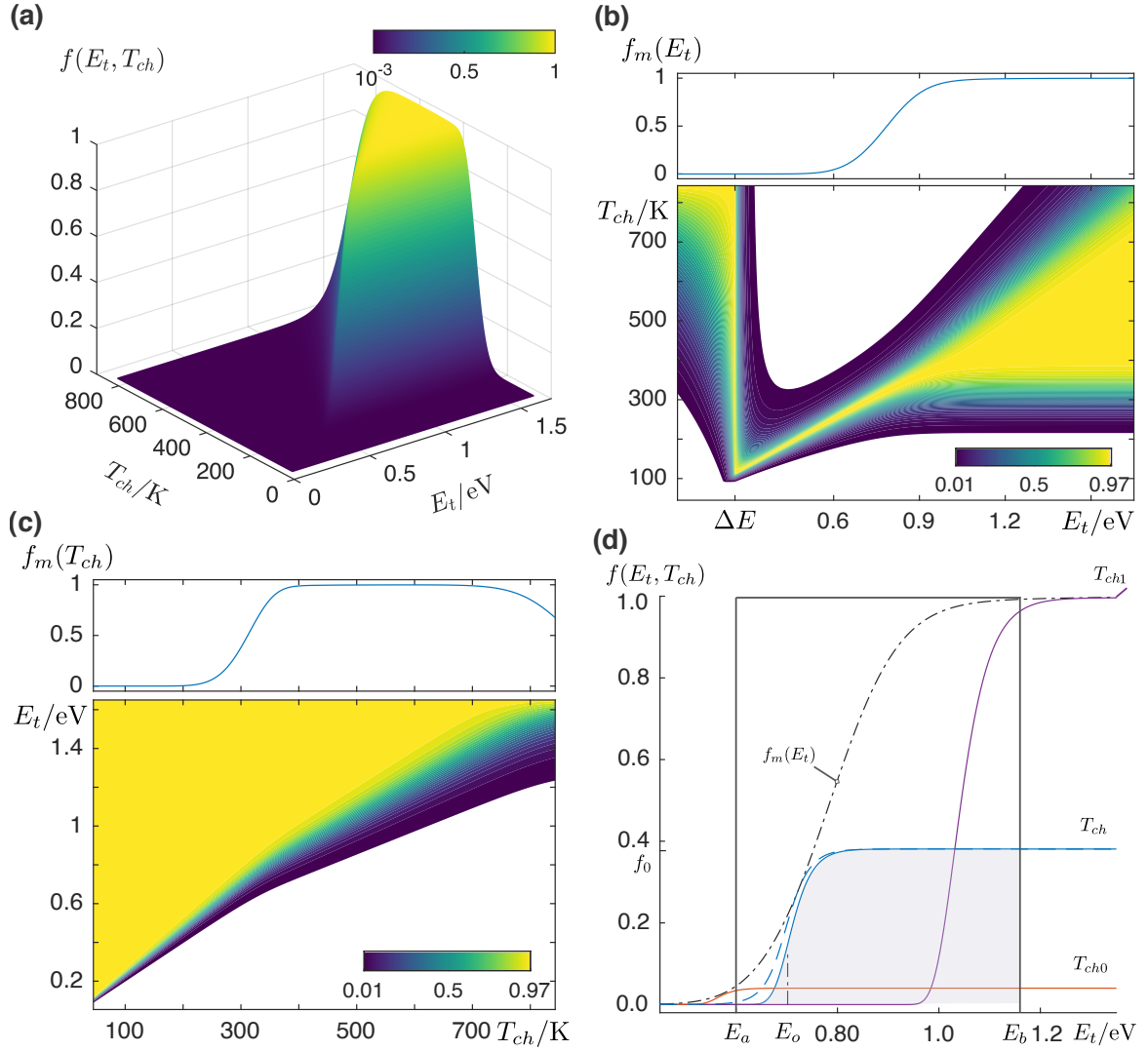


FIG. 2. **The filling function.** (a) The filling function $f(E_t, T_{ch})$ surface. (b) The contour of $f(E_t, T_{ch})_E$, together with $f_m(E_t)$ (top panel), shows a linear relationship between E_t and its optimum charging temperature. (c) The contour plot of $f(E_t, T_{ch})_T$, together with $f_m(T_{ch})$ (top panel), indicates traps cannot be filled at high T_{ch} due to detrapping. (d) The filling function at T_0 (300 K, blue solid line) can be fitted to Eqn. 21, with magnitude $f_m(E_t)$. For a range (E_a, E_b) , the shape of $n(E_t)$ stays the same when $T_{ch} < T_{ch0}$ (250 K), and $f(E_t, T_{ch})_T$ decreases with increasing T_{ch} when $T_{ch} > T_{ch1}$ (450 K). ($I_e = 5 \times 10^{15}$ Hz/cm², $t_{ch} = 10^2$ s, $\Delta E = 0.255$ eV, $\sigma_{abs} = 3 \times 10^{-18}$ cm², $\sigma_{osl} = 10^{-17}$ cm², $v_r = v_t = 10^{10}$ Hz, $k_{rad} = 1.54$ MHz and $A_t = 10^{12}$ Hz.)

(SM [33], section III). To reveal the subtle relationship between E_t and T_{ch} at a given charging condition, we consider the normalized filling functions,

$$f(E_t, T_{ch})_E = f(E_t, T_{ch})/f_m(E_t), \quad (19a)$$

$$f(E_t, T_{ch})_T = f(E_t, T_{ch})/f_m(T_{ch}) \quad (19b)$$

where $f_m(E_t)$ and $f_m(T_{ch})$ are the maximum of $f(E_t, T_{ch})$ for fixed E_t and T_{ch} , respectively. As shown in Fig. 2b, traps can be efficiently charged in a narrow charging temperature range for a fixed trap depth $E_t > \Delta E$. The maximum of filling is given by $f_m(E_t)$, which behaves similar to a logistic function (Fig. 2b top panel). When $E_t < \Delta E$, only at very high temperature can traps be efficiently filled up to a very small $f_m(E_t)$. In these cases, the recombination coefficient $k_{recomb}(E_t, I_e)$ is so huge that the equilibrium of charging is reached within t_{ch} according

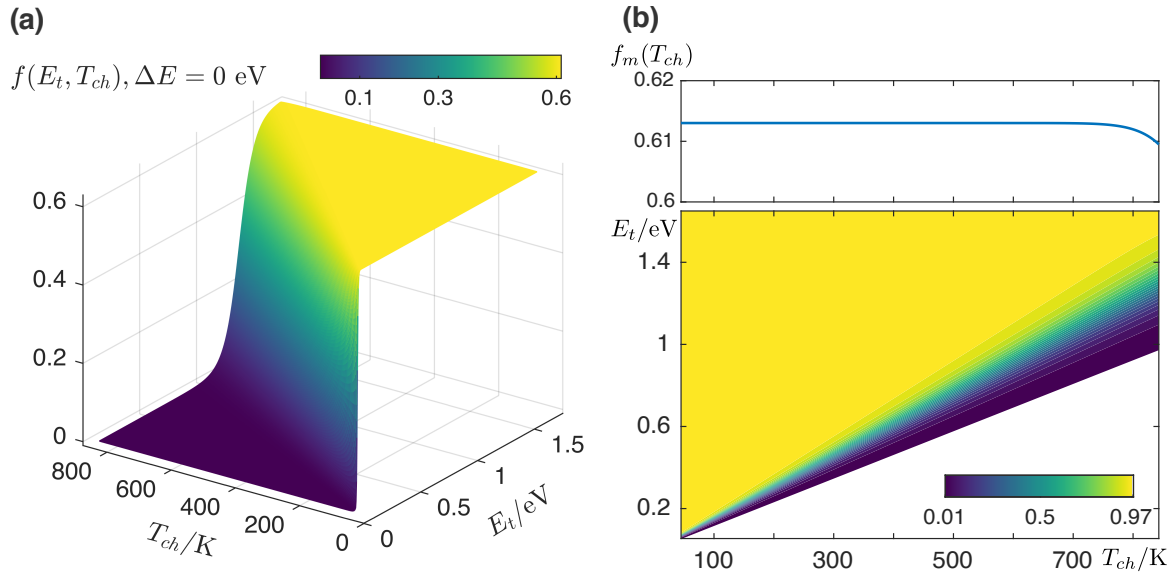


FIG. 3. **The filling function without ΔE .** (a) The filling function $f(E_t, T_{ch})$ surface. (b) The contour plot of $f(E_t, T_{ch})_T$ shows the range where $f(E_t, T_{ch})_T$ changes drastically is linear with charging temperature T_{ch} . The magnitude $f_m(T_{ch})$ is only weakly dependent on temperature T_{ch} . ($I_e = 5 \times 10^{15}$ Hz/cm², $t_{ch} = 10^{-2}$ s, $\Delta E = 0$ eV, $\sigma_{abs} = 3 \times 10^{-18}$ cm², $\sigma_{osl} = 10^{-17}$ cm², $\nu_r = \nu_t = 10^{10}$ Hz, $k_{rad} = 1.54$ MHz and $A_t = 10^{12}$ Hz.)

to Eqn. 6, leading to the relation,

$$f(E_t, T_{ch}) \approx 1 / \left[1 + \frac{\nu_r k_{rad}}{\nu_t \sigma_{abs} I_e} \exp\left(\frac{\Delta E - E_t}{k_B T_{ch}}\right) \right],$$

which reaches its maximum at very high charging temperature T_{ch} . The function $f(E_t, T_{ch})_E$ is fundamental to the understanding of PersL as a function of working temperature. With a trap depth distribution, persistent phosphors often are charged and used at a fixed temperature T_{ch} . In such a case, the filling function $f(E_t, T_{ch})_T$, as in Fig. 2c, predicts a range of trap depths (E_{min}, E_{max}) where the filling function increases dramatically with increasing E_t . Shallow traps ($E_t < E_{min}$) are empty at charging temperature T_{ch} due to severe thermal detrapping. Meanwhile, deep traps ($E_t > E_{max}$) remain essentially filled to $f_m(T_{ch})$ (Fig. 2c) thanks to negligible detrapping. At very high charging temperature T_{ch} , $f_m(T_{ch})$ decreases with increasing T_{ch} because of serious thermal detrapping for deep traps. Both E_{max} and E_{min} are roughly linear with the charging temperature T_{ch} .

The filling function is exactly the initial condition for PersL. The initial condition for TL is at T_0 . This requires a correction factor to the filling function,

$$Q = \exp \left[-\frac{\nu_r}{\beta} \int_{T_{ch}}^{T_0} \exp\left(-\frac{E_t}{k_B T'}\right) dT' \right]. \quad (20)$$

At a fixed charging duration t_{ch} , the filling function just after charging (dashed blue line in Fig. 2d) shows considerable value at shallow traps. These electrons at shallow traps are emptied during the cooling to T_0 eventually. Shown as a solid blue line in Fig. 2d, the filling function at T_0 can be fitted by a double exponential function,

$$f_{ch}(E_t, T_{ch}) = f_0(T_{ch}) \exp \left[-\exp\left(-\frac{E_t - E_o}{k_B(T_{ch} + \Delta T_{ch})}\right) \right]. \quad (21)$$

Here the effective trap depth E_o is the trap depth at which the filling function reaches $f_0(T_{ch}) \exp(-1)$. It is correlated to ΔT_{ch} , and both are dependent on T_{ch} . When $E_t = E_o + 3k_B(T_{ch} + \Delta T_{ch})$, $f_{ch}(E_t, T_{ch})$ approaches $0.9514 \times f_0(T_{ch})$. Clearly, the derivative of $f_{ch}(E_t, T_{ch})$ with respect to E_t has its large value distributed 1-3 $k_B(T_{ch} + \Delta T_{ch})$ around the effective trap depth E_o .

It is interesting to note the shape of trap depth distribution can be preserved when charging is carried out at sufficiently low temperature (indicated as T_{ch0} in Fig. 2d), whose characteristic trap depth E_o is 1-2 $k_B T$ below the minimum of the range, i.e., E_a . The maximum of $f_0(T_{ch})$ as a function of T_{ch} can be found at a charging

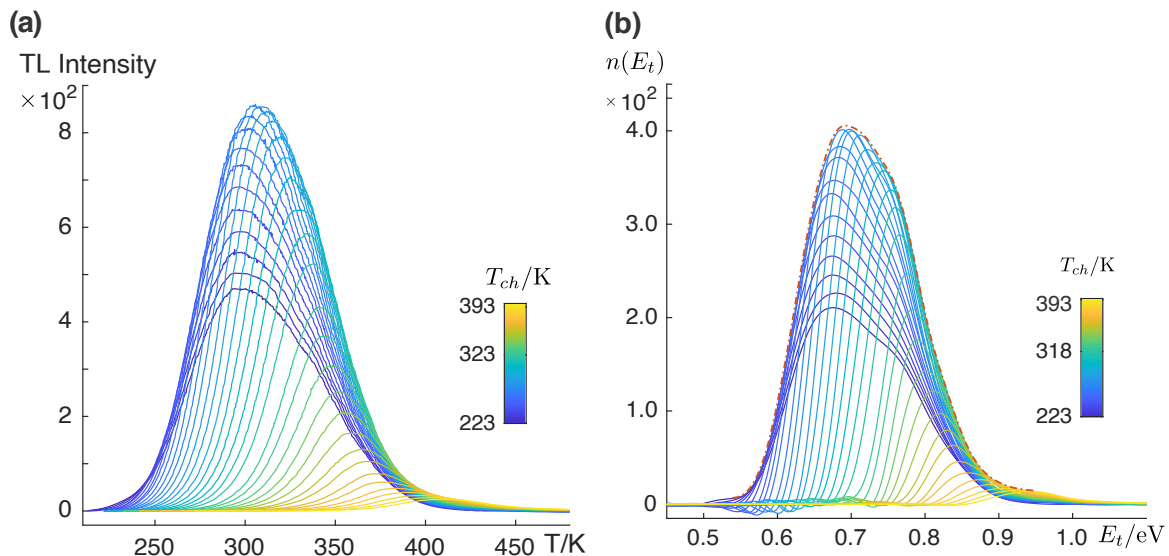


FIG. 4. **The electron population function $n(E_t)$.** The tails of TL profiles (a) and the corresponding electron population profiles (b) of high T_{ch} do not overlap with that of low T_{ch} , suggesting the presence of ΔE . The envelope of $n(E_t)$, i.e. $n(E_t)_{env}$, is shown by an orange dash-line. T_{ch} increases from 223 to 393 K with a step of 5 K. ($t_{ch} = 300$ s, $\beta = 0.5$ K/s, and excitation light $\lambda_{em} = 375$ nm from a LED (50 mA).)

temperature (range) that is high enough to facilitate trapping while suppressing thermal detrapping. When the charging temperature is too high (as indicated by T_{ch1} in Fig. 2d), thermal detrapping becomes dominant so that the maximum of filling function decreases accordingly. The presence of ΔE leads to a temperature range where $f_0(T_{ch})$ is almost independent of T_{ch} (Fig. 2c).

The filling function $f(E_t, T_{ch})$ without ΔE is quite simple, as shown in Fig. 3a. The contour plot of $f(E_t, T_{ch})_T$ clearly shows the effective trap depth E_o (Eqn. 21) is proportional to charging temperature T_{ch} (Fig. 3b). The $f_m(E_t)$ is independent of T_{ch} except at very high temperature (Fig. 3b top panel). Therefore, there exists a lowest temperature $T_{cho} < T_{chi}$ such that the electron population function $n(E_t, T_{cho})$ overlaps with $n(E_t, T_{chi})$ when $E_t > E_{ti} = E_{oi} + 3k_B T_{chi}$. Since electron population functions can be translated into TL curves linearly, this effect also can be observed in TL curves acquired at different charging temperature, while other charging parameters remain fixed. The TL curves of all high charging temperature should overlap with that of the theoretical lowest charging temperature T_{cho} . This has been observed in $\text{LiGa}_5\text{O}_8:\text{Cr}^{3+}$ [6, 47], and the trap depth distribution can then be well probed by the T_m - T_{stop} method [19, 47].

B. The presence of a thermal barrier of charging

If a thermal barrier ΔE is present for charging, the magnitude of filling $f_0(E_t, T_{ch})$ follows $f_m(E_t)$ which increases with increasing E_t . The higher the charging temperature T_{ch} , the higher the percentage the traps with depth E_t are filled as long as T_{ch} is not too high. This can be seen in $\text{BaSi}_2\text{O}_2\text{N}_2:\text{Eu}^{2+}$ as a model phosphor for this study (Fig. 4). The tails of TL curves or $n(E_t, T_{ch})$ for high charging temperature are greater than that of low charging temperature (Fig. 4a,b). The experimental parameters ensure that the shape of $n(E_t, T_{ch})$ does not vary with increasing charging irradiance I_e or charging duration t_{ch} (SM [33], section IV). This clearly indicates the presence of a thermal barrier ΔE . The relative magnitude of charging $f_0(T_{ch})$ (Eqn. 21) can be estimated from the ratio of $n(E_t, T_{ch})$ to $n(E_t, 228$ K), namely,

$$R(E_t)_T = \frac{n(E_t, T_{ch})}{n(E_t, 228 \text{ K})}. \quad (22)$$

We prefer $n(E_t, 228$ K) to $n(E_t, 223$ K) due to its stronger signal and less uncertainties. In Fig. 5a, $R(E_t)_T$ as a function of E_t follows Eqn. 21 evidently when the charging temperature T_{ch} is less than around 283 K. It decreases with increasing E_t when the charging temperature is in the range of (288, 333) K. At even higher charging temperature $T_{ch} > 333$ K, it shows a dip at $E_t \in (0.8, 0.9)$ eV and great oscillation when $E_t \in (0.9, 1.05)$ eV. However, we can

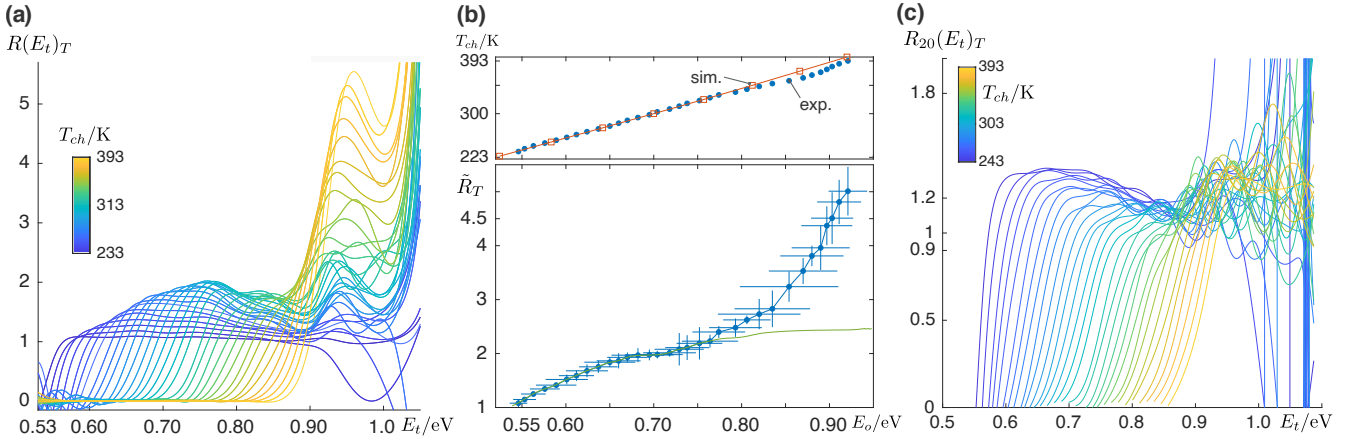


FIG. 5. **Approximating the magnitude of filling function $f_0(T_{ch})$.** (a) The function $R(E_t)_T$ approximates the filling function $f_{ch}(E_t, T_{ch})$ relative to the one obtained at 228 K. (b) As a function of E_o (Eqn. 21), \tilde{R}_T shows big uncertainty when $E_o > 0.85$ eV. E_o agrees well with that obtained from simulation (top panel). The approximated $f_0(T_{ch})$ is shown by the solid green line. (c) The ratio of $R_{20}(E_t)_T$ shows consistency of the filling function at T_{ch} and $T_{ch} - 20$ K. The accumulated errors explains well the large uncertainties of $R(E_t)_T$ at $E_t > 0.85$ eV.

still compress $R(E_t)_T$ into a number \tilde{R}_T , which actually approximates $f_0(T_{ch})$ relative to $f_0(228\text{ K})$. We take the value of $R(E_t)_T$ at $E_t \in (0.65, 0.75)$ eV when $T_{ch} < 293$ K, and the averaged $R(E_t)_T$ in the deep trap range when $T_{ch} \geq 293$ K. Furthermore, the effective trap depths E_o were estimated as well. The plot of \tilde{R}_T against E_o , as shown in Fig. 5b, approximates $f_0(T_{ch})$ for $E_t < \sim 0.80$ eV when the uncertainties are taken into account. As shown in the top panel of Fig. 5b, the effective trap depth E_o agrees quite well with that from a simulation followed by a fitting to Eqn. 21 (SM [33], section V). A slight disagreement appears at $E_t > 0.80$ eV. The dip of $R(E_t)_T$ at $E_t \in (0.8, 0.9)$ eV originates from non-ideality of charging and errors in data processing. We utilize the quantity

$$R_{20}(E_t)_T = \frac{n(E_t, T_{ch})}{n(E_t, T_{ch} - 20\text{ K})} \quad (23)$$

to examine the ratio of two electron populations which have their effective trap depth E_o well separated by a difference of charging temperature as small as possible (20 K here). $R_{20}(E_t)_T$ is shown in Fig. 5c. It should reach a plateau when $E_t > E_o + 3k_B(T_{ch} + \Delta T_{ch})$. After reaching a plateau, however, it slightly decreases with increasing E_t for T_{ch} whose $E_o < 0.75$ eV. This results from the presence of a 'shoulder' in $n(E_t, T_{ch})$ at $E_t \approx 0.75$ eV (Fig. 4b), which originates from the tiny shoulder in the TL profile at ≈ 330 K (Fig. 4a). The oscillation in the range of $E_t \in (0.95, 1.1)$ eV is a consequence of the regularization method which uses oscillatory singular vectors as bases to reconstruct the solution.

C. Extracting the trap depth distribution

The trap distribution can be readily estimated according to,

$$\tilde{N}(E_t) = \frac{n(E_t)_{env}}{f_0(T_{ch})}, \quad (24)$$

given $f_0(T_{ch})$. Here $n(E_t)_{env}$ is the envelope of $n(E_t)$, which actually characterizes the behavior of $n(E_t)$ near the rising edge of $f_{ch}(E_t, T_{ch})$. In this range, the prediction of first-order charging kinetics still holds since $R_{20}(E_t)_T$ stays almost unchanged instead of decreasing with increasing E_t (Fig. 5c). The envelope $n(E_t)_{env}$ is shown as orange dash-dot line in Fig. 4b. However, the quantity $f_0(T_{ch})$ can only be estimated with limited accuracy from Fig. 5b. When $E_o \geq 0.8$ eV, \tilde{R}_T was extrapolated to reach a plateau, mimicking the behavior of $f_m(E_t)$ at large E_t . In this range, both \tilde{R}_T and E_o exhibit large uncertainties. Such uncertainties can be minimized by acquiring highly consistent and accurate TL profiles. Therefore, $f_0(T_{ch})$ is shown in Fig. 5b (bottom panel, green line) as a function of E_o .

The estimated trap distribution $\tilde{N}(E_t)$ is shown in the range of (0.54, 0.95) eV (blue line in Fig. 6a). For a comparison, several $n(E_t, T_{ch})$ ($T_{ch} = 233, 278, 293$ K) were also shown after being scaled to fit the shape of $\tilde{N}(E_t)$.

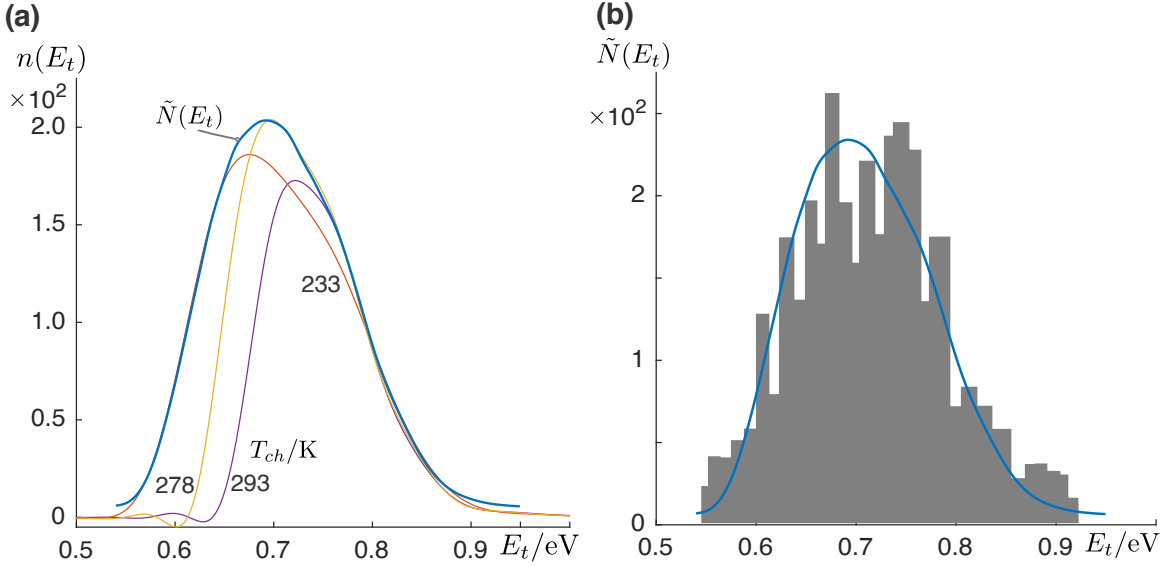


FIG. 6. **Trap depth distribution of BaSi₂O₂N₂:2%Eu²⁺.** (a) The trap distribution $\tilde{N}(E_t)$ (blue) estimated from the envelope $n(E_t)_{env}$. It is compared with scaled $n(E_t, T_{ch})$ for $T_{ch} = 233$ K (orange), 278 K (yellow), and 293 K (purple). (b) The trap distribution obtained by the proposed method (blue solid line, $\times 1.15$) is superior to the one obtained by the method in Ref [21] with correction by $f_0(T_{ch})$ (grey histogram) in terms of precision and resolution.

Clearly, $n(E_t, 233\text{K})$ captures the shape of $\tilde{N}(E_t)$ except in the range of (0.68, 0.78) eV, where the contribution of $n(E_t, T_{ch})$ for $T_{ch} \in (278, 293)$ K dominates. This suggests that the electron population function at the lowest T_{ch} , whose E_o is below the lower limit of trap distribution (E_a), may provide an estimation of the trap depth distribution. In order to obtain high accuracy, the TL curves for each charging temperature T_{ch} must be collected accurately and the signal-noise ratio should be as high as possible.

An alternative method of approximating $\tilde{N}(E_t)$ utilizes the difference between $n(E_t, T_{ch})$ and $n(E_t, T_{ch} + \Delta T)$ in which ΔT is the temperature difference between two neighboring charging temperature T_{ch} . ΔT was 5 K in our experiment. This method is similar to the one proposed by K. Van den Eeckhout et al. in Ref [21]. At first, $n(E_t, T_{ch})$ was corrected by multiplying $1/f_0(T_{ch})$ and then the effective trap depth E_o was estimated. It was assumed that traps with $E_t < E_o$ are completely empty due to thermally detrapping. The average density of trapped electrons in the range $[E_o(T_{ch}), E_o(T_{ch} + \Delta T)]$ is approximated by,

$$\Delta n(E_o) = \frac{1}{\delta E} \int_{E_a}^{E_b} \left[\frac{n(E_t, T_{ch} + \Delta T)}{f_0(T_{ch} + \Delta T)} - \frac{n(E_t, T_{ch})}{f_0(T_{ch})} \right] dE_t,$$

with

$$\delta E = E_o(T_{ch} + \Delta T) - E_o(T_{ch}).$$

The trap depth distribution estimate $\tilde{N}(E_t)$ for $E_t \in (E_o, E_o + \delta E)$ is approximated by $\Delta n(E_o)$, i.e. $\tilde{N}(E_t) \approx \Delta n(E_o)$. It is plotted as a histogram in Fig. 6b, together with the one obtained from $n(E_t)_{env}$ for comparison (solid line Fig. 6b).

Clearly, the shapes of $\tilde{N}(E_t)$ from both methods agree well, but the one obtained via Eqn. 24 offers greater E_t resolution. Therefore, the method of reconstructing trap depth distribution from the envelope of $n(E_t, T_{ch})$ is an excellent method that affords good precision and trap depth resolution.

V. DISCUSSION

Kinetics order. The present method places its validity on first-order kinetics. It implies that trapping or recombination within its corresponding pair is independent from that within other pairs. In the present model, the electron at the excited state of a trap only retraps into its ground state. We ignore its trapping into a nearby empty trap regardless of the trap depth. The model requires the NN distance of an electron-trap pair or electron-hole pair be

much smaller than the average distance between pairs, such that electron transitions among pairs are negligible. This is often satisfied for persistent phosphor under laboratory conditions. Retrapping among traps would bring reshuffle of trapped electrons. This effect can be clearly detected when the density of electrons at the excited states of traps is increased significantly via stimulation by light [48–50] or even by mechanical stress [28]. In cases of isothermal detrapping alone, i.e., delaying the phosphor at T_{ch} , such effect is not prominent due to small density of electrons at the excited states of traps. This is confirmed by the fact that the filling function does not increase with increasing waiting time in BaSi₂O₂N₂: 2%Eu²⁺ phosphor (SM [33], section VI).

We now compare the first-order kinetics of local model with the global model of electron transition. The local model provides a more convenient framework than the global model when global retrapping is not important. The excited state of a trap is the conduction band (CB) state in global model. The delocalized CB electrons have freedom to retrap into traps with coefficient k_t or to recombine with holes with coefficient k_r , according to the kinetic law of mass action [51]. However, the effect due to these global electron transition can be inferred from the filling function $f(E_t, t, q)$. According to the global model, $f(E_t, t, q)$ follows the ordinary differential equation [52],

$$\frac{\partial f(E_t, t, q)}{\partial t} = -k_r \exp\left(-\frac{E_t}{k_B T}\right) f(E_t, t, q) + k_t n_c(t) [1 - f(E_t, t, q)], \quad (25)$$

where $n_c(t)$ is the density of CB electrons. In cases of an isothermal stimulation, Eqn. 25 suggests that the filling function $f(E_t, t, q)$ starts to increase with increasing delaying time t_0 for traps where the trapping rate outweighs the thermal detrapping rate. This is an indication of strong global retrapping, but it has not been firmly supported by experimental observation. The TL due to an electron population function $n(E_t, t, q)$ is given by [32, 52],

$$I(t) = \frac{m(t)k_r}{(N_0 - n(t))k_t + m(t)k_r} \int_0^\infty k_r \exp\left(-\frac{E_t}{k_B T}\right) n(E_t, t, q) dE_t, \quad (26)$$

upon assuming that $n_c(t)$ is a slowly varying function and $k_t \leq k_r$. Here $m(t)$ is the density of holes, while $n(t) = \int_0^\infty n(E_t, t, q) dE_t$ is the total density of trapped electrons. When global retrapping is absent ($k_t = 0$), the kinetics is of first-order. A trap depth distribution may produce certain PersL asymptotes [53, 54], but its numerical simulation appeared just recently [22, 55]. The second-order kinetics requires $k_r = k_t$. In this case, trapped electrons are delayed further to recombine with holes due to retrapping. Hence, the global model differs from the local model by whether to assign excited state electrons to their nearby holes. Global reshuffling of electron population cannot be ignored when $n_c(t)$ is greatly enhanced by external stimulation. For example, mechanical stimulation to BaSi₂O₂N₂:2%Eu²⁺ phosphor increases $n_c(t)$ (according to the global model), and these delocalized electrons retrap into deep traps (Eqn. 25) indeed [28]. For persistent luminescence or thermoluminescence, $n_c(t)$ is limited by relatively deep traps in these materials.

Therefore, when global retrapping is not prominent, the first-order kinetics from the local model already provides a clear physics picture and convenient mathematical tools to describe thermoluminescence from a distribution of trap depth.

Uncertainty of trap depth distribution. We have proposed to extract the trap depth distribution from the envelope of the electron population function obtained at different charging temperatures. The method enjoys high precision and resolution in trap depth. The uncertainties come from both the accuracy of TL curves and the regularization method. TL curves at different T_{ch} should be obtained in a very consistent manner and the signal-noise ratio should be high. The reason is that $f_0(T_{ch})$, where much uncertainties originate, is required to correct for $n(E_t)$ profiles. Furthermore, the envelope also depends on accurate $n(E_t)$. In addition to using optical detectors that provide high sensitivity and dynamic range, increasing charging duration and the intensity of charging light also helps to obtain TL curves of strong signal. The dark background must be collected carefully to produce a correct net TL curve. Moreover, it is a good practice to record a measurement with identical conditions as the first one in a long series of TL experiments, in order to assess phosphor or light source degradation. The regularization method utilizes general singular values and the corresponding oscillatory singular vectors to reconstruct the solution. It gives smooth approximated solutions even when the true solution shows discontinuity. As noises in experimental TL curves will be magnified in the electron population function, the signal-noise ratio should be high enough to avoid oscillatory behavior in the solution.

The accuracy of the method depends on the frequency factor ν_r , which is correlated with the trap depth E_t via the Boltzmann factor. However, the extracted trap depth E_t is almost a linear function of T at fixed ν_r , and it scales approximately with $\ln(\nu_r)$ for a fixed T (SM [33], section II). Inaccurate ν_r shifts and distorts the trap depth distribution slightly. Several methods have been proposed to extract ν_r according to the global model without a trap depth distribution [37, 56]. The other alternative goes to first calculating E_t accurately with advanced ab initio methods and then determining ν_r accordingly.

Extending the method to complicated materials. The present model assumes the presence of only one luminescent center and only one thermal barrier. Real persistent phosphors can have multiple luminescent centers

or one kind of luminescent center at multiple crystallographic sites, each providing its own emission spectrum and thermal barrier. In these cases, the first-order kinetics must be applied to each distinctive trapping-recombination processes independently and the output is the sum of these independent processes due to the validity of superposition principle. It is noteworthy that the recording of the TL intensity should be spectrally resolved to distinguish the contribution of recombination processes.

Importance of trap distribution. The trap distribution $\tilde{N}(E_t)$ can be compared across persistent phosphors given the frequency factor ν_r . Actually, the exact value of ν_r is not import for the purpose of understanding the behaviors of persistent phosphors. Given an estimated ν_r , it is easy to simulate the decay profile for PersL or the TL profiles for different charging and working conditions from the trap depth distribution.

Trap depth distributions have found many ways in technological applications. The obvious one is to understand and tune the behavior PersL of persistent phosphors. For example, the trap depth distribution in garnet phosphors can be tuned by band engineering to optimize optical storage properties [57]. Furthermore, it provides an estimation of the optimum charging and working temperature (T_{opt}) of persistent phosphor. The integrated output of PersL originates from integrating $n(E_t)$ for $E_t \in [k_B T_{ch} \ln(\nu_r t_1), k_B T_{ch} \ln(\nu_r t_2)]$, where t_1 and t_2 are the delay time after charging ($t_1 \approx 1$ s). The optimum temperature T_{opt} can be found via seeking T_{ch} such that its maximum of $n(E_t, T_{ch})$ matches the maximum of $N(E_t)$. For the model phosphor $\text{BaSi}_2\text{O}_2\text{N}_2:2\%\text{Eu}^{2+}$, the T_{opt} is around 278 K (Fig. 6). More importantly, a deeper understanding of persistent phosphors is achievable when trap depth distributions can be used for machine learning to reveal hidden laws.

VI. CONCLUSION

In this contribution, a method was proposed to extract trap distribution from TL curves with the presence of a thermal barrier of charging. It is based on a local transition model that leads to first-order kinetics of charge transitions. The model predicts the evolution of charging magnitude as a function of charging temperature. Within this framework, the electron population was reconstructed by regularization method from TL curves. Firstly, the electron population function $n(E_t, T_{ch})$ was converted from the corresponding TL curves with various charging temperature T_{ch} and other charging parameters fixed. Secondly, the relative magnitude of the filling function, i.e., $f_0(T_{ch})$, is estimated according to the first-order kinetics. Then, the envelope of the $n(E_t, T_{ch})$ for all T_{ch} , i.e. $n(E_t)_{env}$ is constructed accordingly. Finally, the trap depth distribution can be estimated according to $\tilde{N}(E_t) = n(E_t)_{env}/f_0(T_{ch})$ (Eqn. 24).

The method yields high resolution in trap depth, and it can provide good precision when TL curves have high signal strength and high signal-noise ratio. The trap distribution definitely promotes the understanding and tailoring of the properties of persistent phosphors.

ACKNOWLEDGMENTS

Ang Feng and Philippe F. Smet acknowledge the financial support from Ghent University via the GOA-Enclose project. Jiaren Du acknowledges the financial support of the BOF postdoctoral fellowship (No. BOF20/PDO/015) from Ghent University.

-
- [1] K. Van den Eeckhout, P. F. Smet, and D. Poelman, Persistent luminescence in Eu^{2+} -doped compounds: A review, *Materials* **3**, 2536 (2010).
 - [2] K. Van den Eeckhout, D. Poelman, and P. Smet, Persistent luminescence in non- Eu^{2+} -doped compounds: A review, *Materials* **6**, 2789 (2013).
 - [3] J. Xu and S. Tanabe, Persistent luminescence instead of phosphorescence: History, mechanism, and perspective, *J. Lumin.* **205**, 581 (2019).
 - [4] P. F. Smet, K. Van den Eeckhout, O. Q. De Clercq, and D. Poelman, Chapter 274 - persistent phosphors, in *Including Actinides*, Handbook on the Physics and Chemistry of Rare Earths, Vol. 48, edited by J.-C. Bünzli and V. K. Pecharsky (Elsevier, 2015) pp. 1–108.
 - [5] J. Du, O. De Clercq, and D. Poelman, Temperature dependent persistent luminescence: Evaluating the optimum working temperature, *Sci. Rep.* **9**, 10517 (2019).
 - [6] J. Du, A. Feng, and D. Poelman, Temperature dependency of trap-controlled persistent luminescence, *Laser Photonics Rev.* **14**, 2000060 (2020).
 - [7] A. Y.-T. Wang, R. J. Murdock, S. K. Kauwe, A. O. Oliynyk, A. Gurlo, J. Brgoch, K. A. Persson, and T. D. Sparks, Machine learning for materials scientists: An introductory guide toward best practices, *Chem. Mater.* **32**, 4954 (2020).

- [8] D. Van der Heggen, J. Joos, D. Rodríguez Burbano, J. Capobianco, and P. Smet, Counting the photons: Determining the absolute storage capacity of persistent phosphors, *Materials* **10**, 867 (2017).
- [9] C. Tydtgat, K. W. Meert, D. Poelman, and P. F. Smet, Optically stimulated detrapping during charging of persistent phosphors, *Opt. Mater. Express* **6**, 844 (2016).
- [10] D. Van der Heggen, J. J. Joos, and P. F. Smet, Importance of evaluating the intensity dependency of the quantum efficiency: Impact on leds and persistent phosphors, *ACS Photonics* **5**, 4529 (2018).
- [11] J. Botterman, J. J. Joos, and P. F. Smet, Trapping and detrapping in $\text{SrAl}_2\text{O}_4:\text{Eu}$, Dy persistent phosphors: Influence of excitation wavelength and temperature, *Phys. Rev. B* **90**, 085147 (2014).
- [12] P. F. Smet, K. Van den Eeckhout, A. J. Bos, E. v. der Kolk, and P. Dorenbos, Temperature and wavelength dependent trap filling in $\text{M}_2\text{Si}_5\text{N}_8:\text{Eu}$ ($\text{M}=\text{Ca},\text{Sr},\text{Ba}$) persistent phosphors, *J. Lumin.* **132**, 682 (2012).
- [13] R. Chen, On the calculation of activation energies and frequency factors from glow curves, *J. Appl. Phys.* **40**, 570–585 (1969).
- [14] P. Kivits and H. Hagebeuk, Evaluation of the model for thermally stimulated luminescence and conductivity; reliability of trap depth determinations, *J. Lumin.* **15**, 1 (1977).
- [15] G. F. J. Garlick and A. F. Gibson, The electron trap mechanism of luminescence in sulphide and silicate phosphors, *Proc. Phys. Soc.* **60**, 574 (1948).
- [16] A. C. Coleman and E. G. Yukihara, On the validity and accuracy of the initial rise method investigated using realistically simulated thermoluminescence curves, *Radiat. Meas.* **117**, 70 (2018).
- [17] H. Gobrecht and D. Hofmann, Spectroscopy of traps by fractional glow technique, *J. Phys. Chem. Solids* **27**, 509 (1966).
- [18] A. Chruścińska, The fractional thermoluminescence: some aspects concerning the experimental data analysis, *J. Lumin.* **62**, 115 (1994).
- [19] S. W. S. McKeever, On the analysis of complex thermoluminescence glow-curves: Resolution into individual peaks, *Phys. Status Solidi A* **62**, 331 (1980).
- [20] F. Urbach, Zur lumineszenz der alkalihalogenide, *Sitzungsberichte Akad. der Wiss. Wien* **139**, 363 (1930).
- [21] K. Van den Eeckhout, A. J. J. Bos, D. Poelman, and P. F. Smet, Revealing trap depth distributions in persistent phosphors, *Phys. Rev. B* **87**, 045126 (2013).
- [22] V. M. Khanin, I. I. Vruble, R. G. Polozkov, I. A. Shelykh, I. D. Venevtsev, A. Meijerink, H. Wiczorek, J. Boerekamp, S. Spoor, P. A. Rodnyi, and C. Ronda, Modeling and assessment of afterglow decay curves from thermally stimulated luminescence of complex garnets, *J. Phys. Chem. A* **123**, 1894 (2019).
- [23] P. Dorenbos, Thermal quenching of Eu^{2+} 5d-4f luminescence in inorganic compounds, *J. Phys.: Condens. Matter* **17**, 8103 (2005).
- [24] E. Mihóková and M. Nikl, Luminescent materials: Probing the excited state of emission centers by spectroscopic methods, *Meas. Sci. Technol.* **26**, 012001 (2014).
- [25] J. Botterman, K. V. den Eeckhout, A. J. J. Bos, P. Dorenbos, and P. F. Smet, Persistent luminescence in $\text{MSi}_2\text{O}_2\text{N}_2:\text{Eu}$ phosphors, *Opt. Mater. Express* **2**, 341 (2012).
- [26] A. Feng and P. F. Smet, A review of mechanoluminescence in inorganic solids: Compounds, mechanisms, models and applications, *Materials* **11**, 484 (2018).
- [27] J. Botterman, K. V. den Eeckhout, I. D. Baere, D. Poelman, and P. F. Smet, Mechanoluminescence in $\text{BaSi}_2\text{O}_2\text{N}_2:\text{Eu}$, *Acta Mater.* **60**, 5494 (2012).
- [28] R. R. Petit, S. E. Michels, A. Feng, and P. F. Smet, Adding memory to pressure-sensitive phosphors, *Light Sci. Appl.* **8**, 124 (2019).
- [29] V. Bachmann, C. Ronda, O. Oeckler, W. Schnick, and A. Meijerink, Color point tuning for $(\text{Sr},\text{Ca},\text{Ba})\text{Si}_2\text{O}_2\text{N}_2:\text{Eu}^{2+}$ for white light leds, *Chem. Mater.* **21**, 316 (2009).
- [30] B.-G. Yun, T. Horikawa, H. Hanzawa, and K.-i. Machida, Preparation and luminescence properties of single-phase $\text{BaSi}_2\text{O}_2\text{N}_2:\text{Eu}^{2+}$, a bluish-green phosphor for white light-emitting diodes, *J. Electrochem. Soc.* **157**, J364 (2010).
- [31] X.-Y. Sun, Z.-P. Ye, Y.-T. Wu, P. Gao, R.-H. Mao, Z.-J. Zhang, and J.-T. Zhao, A simple and highly efficient method for synthesis of Ce^{3+} -activated borogermanate scintillating glasses in air, *J. Am. Ceram. Soc.* **97**, 3388 (2014).
- [32] A. Feng, S. Michels, A. Lamberti, W. Van Paeppegem, and P. F. Smet, Relating structural phase transitions to mechanoluminescence: The case of the $\text{Ca}_{1-x}\text{Sr}_x\text{Al}_2\text{Si}_2\text{O}_8:1\%\text{Eu}^{2+},1\%\text{Pr}^{3+}$ anorthite, *Acta Mater.* **183**, 493 (2020).
- [33] See supplemental material at <http://link.aps.org/supplemental/10.1103/PhysRevB> for additional information on thermal quenching profiles, the implementation of regularization method in MATLAB, does dependency of the electron population function, the values of parameters for simulation, the simulated effective trap depth for different charging temperature and the electron population function at various delay time. It includes Refs [10, 28, 29, 32, 37, 45, 46, 49, 58, 59].
- [34] T. Aitasalo, J. Hölsä, H. Jungner, M. Lastusaari, and J. Niittykoski, Thermoluminescence study of persistent luminescence materials: Eu^{2+} - and R^{3+} -doped calcium aluminates, $\text{CaAl}_2\text{O}_4:\text{Eu}^{2+},\text{R}^{3+}$, *J. Phys. Chem. B* **110**, 4589 (2006).
- [35] J. J. Joos, K. Korthout, L. Amidani, P. Glatzel, D. Poelman, and P. F. Smet, Identification of $\text{Dy}^{3+}/\text{Dy}^{2+}$ as electron trap in persistent phosphors, *Phys. Rev. Lett.* **125**, 033001 (2020).
- [36] T. Lyu and P. Dorenbos, Towards information storage by designing both electron and hole detrapping processes in bismuth and lanthanide-doped $\text{LiRE}(\text{Si},\text{Ge})\text{O}_4$ ($\text{RE} = \text{Y}, \text{Lu}$) with high charge carrier storage capacity, *Chem. Eng. J.* **400**, 124776 (2020).
- [37] J. T. Randall, M. H. F. Wilkins, and M. L. E. Oliphant, Phosphorescence and electron traps I. The study of trap distributions, *Proc. R. Soc. Lond. A* **184**, 365 (1945).
- [38] J. T. Randall and M. H. F. Wilkins, Phosphorescence and electron traps II. The interpretation of long-period phosphorescence, *Proc. R. Soc. Lond. A* **184**, 390 (1945).

- [39] J. H. Flynn, The "temperature integral" - Its use and abuse, *Thermochim. Acta* **300**, 83 (1997).
- [40] J. J. M. Órfão, Review and evaluation of the approximations to the temperature integral, *AIChE J.* **53**, 2905 (2007).
- [41] M. Balarin, Improved approximations of the exponential integral in tempering kinetics, *J. Therm. Anal.* **12**, 169 (1977).
- [42] A. N. Tikhonov and V. Y. Arsenin, *Solutions of ill-posed problems*, Scripta series in mathematics (Winston; distributed solely by Halsted Press, Washington: New York, USA, 1977).
- [43] P. C. Hansen, *Discrete Inverse Problems* (Society for Industrial and Applied Mathematics, Philadelphia, USA, 2010).
- [44] P. C. Hansen and D. P. O'Leary, The use of the l-curve in the regularization of discrete ill-posed problems, *SIAM J. Sci. Comput.* **14**, 1487 (1993).
- [45] P. C. Hansen, Regularization Tools: A Matlab package for analysis and solution of discrete ill-posed problems, *Nume. Algor.* **6**, 1 (1994).
- [46] P. C. Hansen, Regularization Tools version 4.0 for Matlab 7.3, *Numer. Algor.* **46**, 189 (2007).
- [47] O. Q. De Clercq, J. Du, P. F. Smet, J. J. Joos, and D. Poelman, Predicting the afterglow duration in persistent phosphors: A validated approach to derive trap depth distributions, *Phys. Chem. Chem. Phys.*
- [48] P. Avouris and T. N. Morgan, A tunneling model for the decay of luminescence in inorganic phosphors: The case of $\text{Zn}_2\text{SiO}_4\text{:Mn}$, *J. Chem. Phys.* **74**, 4347 (1981).
- [49] W. Jia, H. Yuan, S. Holmstrom, H. Liu, and W. Yen, Photo-stimulated luminescence in $\text{SrAl}_2\text{O}_4\text{:Eu}^{2+}, \text{Dy}^{3+}$ single crystal fibers, *J. Lumin.* **83-84**, 465 (1999).
- [50] D. Van der Heggen, D. Vandenberghe, N. K. Moayed, J. De Grave, P. F. Smet, and J. J. Joos, The almost hidden role of deep traps when measuring afterglow and thermoluminescence of persistent phosphors, *J. Lumin.* **226**, 117496 (2020).
- [51] E. Kotomin and V. Kuzovkov, eds., *Modern Aspects of Diffusion-Controlled Reactions*, Comprehensive Chemical Kinetics, Vol. 34 (Elsevier, 1996) pp. 1 – 52.
- [52] R. Chen and S. W. S. McKeever, *Theory of Thermoluminescence and Related Phenomena* (World Scientific, Singapore, 1997).
- [53] W. F. Hornyak and R. Chen, Thermoluminescence and phosphorescence with a continuous distribution of activation energies, *J. Lumin.* **44**, 73 (1989).
- [54] M. N. Berberan-Santos, E. N. Bodunov, and B. Valeur, Luminescence decays with underlying distributions of rate constants: General properties and selected cases, in *Fluorescence of Supramolecules, Polymers, and Nanosystems*, Vol. 4, edited by M. N. Berberan-Santos (Springer Berlin Heidelberg, Berlin, Heidelberg, 2007) pp. 67–103.
- [55] V. M. Khanin, I. I. Vruble, R. G. Polozkov, I. D. Venevtsev, P. A. Rodnyi, T. Tikhvatulina, K. Chernenko, W. Drozdowski, M. E. Witkowski, M. Makowski, E. V. Dorogin, N. V. Rudin, C. Ronda, H. Wiczorek, J. Boerekamp, S. Spoor, I. A. Shelykh, and A. Meijerink, Complex garnets: Microscopic parameters characterizing afterglow, *J. Phys. Chem. C* **123**, 22725 (2019).
- [56] V. Khanin, I. Venevtsev, S. Spoor, J. Boerekamp, A.-M. van Dongen, H. Wiczorek, K. Chernenko, D. Buettner, C. Ronda, and P. Rodnyi, A new method for unambiguous determination of trap parameters from afterglow and TSL curves connection: Example on garnets, *Opt. Mater.* **72**, 161 (2017).
- [57] W. Li, Y. Zhuang, P. Zheng, T.-L. Zhou, J. Xu, J. Ueda, S. Tanabe, L. Wang, and R.-J. Xie, Tailoring trap depth and emission wavelength in $\text{Y}_3\text{Al}_{5-x}\text{Ga}_x\text{O}_{12}\text{:Ce}^{3+}, \text{V}^{3+}$ phosphor-in-glass films for optical information storage, *ACS Appl. Mater. Interfaces* **10**, 27150 (2018).
- [58] R. Iacono and J. P. Boyd, New approximations to the principal real-valued branch of the lambert W -function, *Adv. Comput. Math* **43**, 1403 (2017).
- [59] N. F. Mott, On the absorption of light by crystals, *Proc. R. Soc. London, Ser. A* **167**, 384 (1938).

Supplemental Material:

Extracting trap depth distributions in persistent phosphors with a thermal barrier for charging

Ang Feng,^{1,2} Jiaren Du,^{1,2} and Philippe F. Smet^{1,2,*}

¹*Lumilab, Department of Solid State Sciences, Faculty of Sciences,
Ghent University, Krijgslaan 281-S1, Ghent 9000, Belgium*

²*Center for Nano- and Biophotonics (NB-Photonics), Ghent University, Belgium*

(Dated: June 3, 2022)

I. THERMAL QUENCHING PROFILES

In a normal thermal quenching (TQ) experiment, the phosphor was heated from low temperature to high temperature continuously at a fixed rate while being excited by light (charging). The integrated intensity of the emission spectra as a function of temperature is thus called the TQ profile. The electron trapping in persistent phosphors leads to reduced emission intensity. Therefore, we adopt the method from Ref [32]. The charging protocol (Fig. S1a) characterizes charging at multiple T for 30 s during heating from 213 to 498 K. The spectrum of each charging temperature T was obtained by averaging five spectra from the 24-28th s of the charging. Each of these spectra (Fig. S1b) was integrated 400 nm to 650 to calculate the emission intensity $I_t(T)$. Then, $I_t(T)$ was normalized with respect to $I_t(213\text{ K})$, leading to the TQ profile $I_q(T)$.

The TQ profile (Fig. S1c) was fitted to the single-barrier model [59],

$$I_q(T) = \frac{I_0}{1 + A \exp\left(-\frac{E_q}{k_B T}\right)}, \quad (\text{S1})$$

where E_q is the thermal barrier and k_B the Boltzmann constant. I_0 and A are fitting parameters. The fitting results give $I_0 = 0.9676$, $A = 289.4$ and the thermal barrier $E_q = 254.1\text{ meV}$.

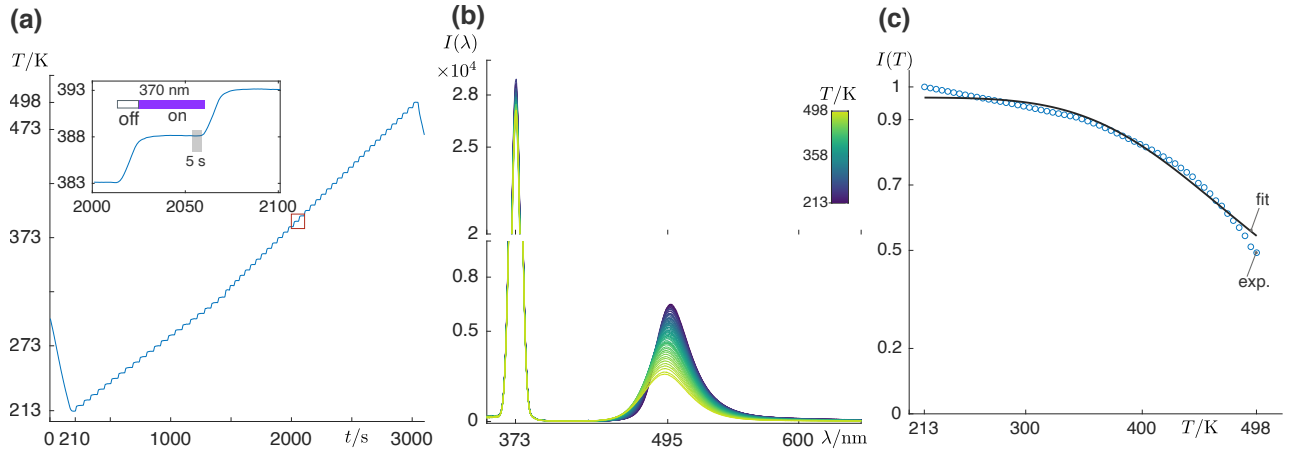


FIG. S1. **Thermal quenching profiles.** (a) The phosphor was warmed up from 213 to 498 K, but it was charged for 30 s at multiple temperature T from 213 to 498 K with a step of 5 K. Five spectra from the 24-28th s was averaged to $I(\lambda)$ (shown in the inset). (b) With increasing T , the intensity of the spectra of excitation light decreases only slightly while that of the emission spectra of $\text{BaSi}_2\text{O}_2\text{N}_2:2\%\text{Eu}^{2+}$ decreases significantly. (c) The integrated emission intensity (400-650 nm) was normalized to that of $T = 213\text{ K}$, and was then fitted to the single barrier model $I_q(T) = I_0 / \left[1 + A \exp\left(-\frac{E_q}{k_B T}\right) \right]$. The thermal barrier is found to be $E_q = 0.254\text{ eV}$.

* philippe.smet@UGent.be

A generalized singular value decomposition (GSVD) method is utilized to decompose K and L simultaneously so that the solution is given by,

$$n_{L,\lambda} = \sum_{k=1}^N \phi_k^{[L,\lambda]} \frac{u_k'^T i}{\sigma_k'} n_k', \quad (\text{S9})$$

where the ratio σ_k'/μ_k' (with $\sigma_k'^2 + \mu_k'^2 = 1$) is the generalized singular values. The right singular vectors n_k' , which are shared by both L and A , are mutually independent but are neither normalized nor orthogonal. There are two sets of left GSVD orthonormal vectors u_k' and v_k' satisfy

$$K n_k' = \sigma_k' u_k', \quad L n_k' = \mu_k' v_k'.$$

Here we provide the MATLAB code that solves $n(E_t)$ from TL data. We utilize *Regularization Tools* MATLAB package by Per Christian Hansen [45, 46]. We assume the package has been added to the search path of MATLAB.

- Discretization.

```
kB = 0.08617; nu = 1e10; beta = 0.5; N = 1600;
Ea = 300; Eb = 1200; T0 = 213.15; Tm = 473.15; de = (Eb-Ea)/N; dT = (Tm-T0)/
N; % The units of Ea and Eb are meV.
e = Ea+(0.5:N-0.5)'*de; t = T0+(0.5:N-0.5)'*dT; [E,T] = meshgrid(e,t);
Kf = @(x,y) de*nu/beta*exp(-x./(kB*y)-nu/beta*kB*y.^2./x.*exp(-x./(kB*y))./
sqrt(1+4*kB*y./x));
K1 = Kf(E,T); K2 = Kf(2*Eb-E,T); K3 = Kf(2*Ea-E,T);
zIdx = (2*Ea-E)<0; K3(zIdx) = 0; K = K1+K2+K3;
L = diag([-1;ones(N-2,1)*(-2);-1]);
L(2:N,1:N-1) = L(2:N,1:N-1)+diag(ones(N-1,1));
L(1:N-1,2:N) = L(1:N-1,2:N)+diag(ones(N-1,1));
```

In Fig. S3, the kernel $K(E_t, T)$ at large E_t and large T is larger than expected due to the reflexive boundary condition.

- GSVD.

```
[U,sm,X,V,W] = cgsvd(K,L).
```

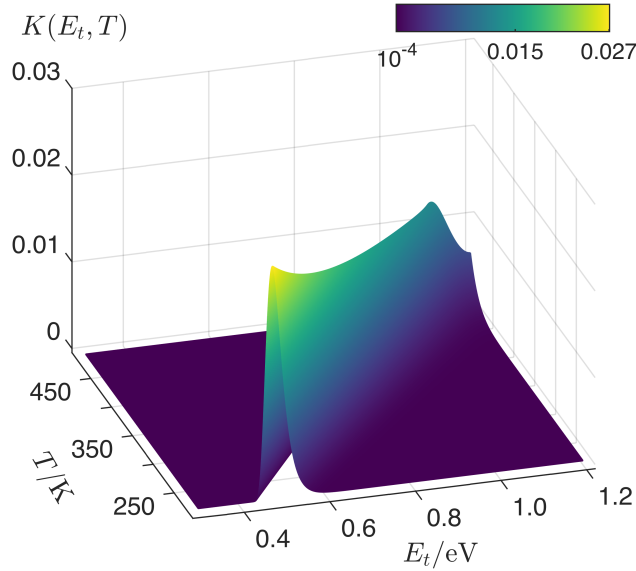


FIG. S3. **The regularization kernel.** The kernel $K(E_t, T)$ (Eqn S7) with reflexive boundary shown in $[E_a, E_b] \times [T_0, T_m]$. Note $\nu_r = 10^{10}$ Hz, $\beta = 0.5$ K/s and $k_B = 0.08617$ meV.

- Denoise TL signal. The TL signal is denoised by 1d stationary wavelet transform (1d SWT) and then interpolated to a uniform temperature range.

```
TLt = TL(:,1)+273.15; TLint = TL(:,2);
TLint_den = wdenoise(TLint); % The TL signal was first denoised via wavelet.
```

The signal `TLint_den` was further denoised by 1d SWT via the Wavelet Analyzer APPs of MATLAB. The cleaned signal is saved as `TLintp`, which will be interpolated to the temperature vector `t`.

```
b = interp1(TLt,TLintp,t,'spline');
```

- Choose λ_{opt} . The optimized regularization parameter λ_{opt} can be found from the corner of the L-curve which can be calculated from GSVD of the problem. This involves solving Eqn. S6 by a series of sampled parameters via the `l_curve` function,

```
[lambda_opt,~,~,reg_param] = l_curve(U,sm,b,'Tikh',L,V);
```

where the desired parameter λ_{opt} is `lambda_opt`.

- Solve \mathbf{x}_λ . The optimal solution can be calculated by the filtering algorithm according to Eqn S9, by calling the `tikhonov` function,

```
[x_lambda,rho,eta] = tikhonov(U,sm,X,b,lambda_opt);
```

which gives `x_lambda`, and additionally the solution norm `rho` and residual norm `eta`.

The recombination rate coefficient ν_r in the kernel (Eqn S3) has been fixed to 10^{10} Hz in the regularization method. To vary ν_r only slightly alters the value of trap depth, which scales approximately with $\ln(\nu_r)$. The TL intensity at temperature T comes from $n(E_t)$ when E_t is only a 1-3 $k_B T$ around the effective trap depth E_s ,

$$E_s = k_B T W(\nu_r T / \beta). \quad (\text{S10})$$

Here $W(\cdot)$ is the Lambert W function of the 0 branch and β the heating rate. As shown in Fig. S4, E_s is almost a linear function of T at fixed ν_r (bottom panel) and it scales approximately with $\log_{10}(\nu_r)$. This is understandable

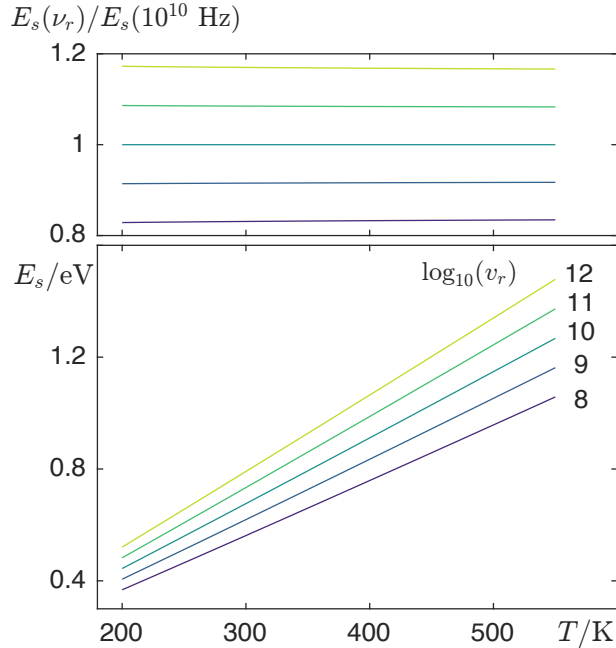


FIG. S4. E_s - ν_r relationship. The effective trap depth of $E_s(T)$ is almost a linear function of T (bottom panel). It scales roughly with $\ln(\nu_r)$ (top panel).

from the asymptotic expansion of the Lambert W function, i.e., $W(x) \approx \ln(x) - \ln[\ln(x)]$ [58]. At large argument x , the derivative of $W(x)$, i.e., $W'(x) \approx [1 - 1/\ln(x)]/x$, is actually around 0. For a scalar factor a of x , we have,

$$\frac{W(ax)}{W(x)} \approx 1 + \frac{\ln(a)(1 - 1/\ln(x))}{W(x)} \quad (\text{S11a})$$

$$\approx 1 + \phi \ln(a), \quad (\text{S11b})$$

in which ϕ is a slowly varying function of x , which can be reckoned as a constant accordingly.

III. PARAMETERS FOR THE SIMULATIONS

The parameters for simulations are estimated from $\text{BaSi}_2\text{O}_2\text{N}_2:\text{Eu}^{2+}$ or given as empirical values that are in reasonable ranges. The spontaneous emission rate coefficient k_{rad} of Eu^{2+} is the inverse of decay time at low temperature (65 ns) [29]. The thermal barrier ΔE is obtained from the thermal quenching data (section I). The absorption cross section of Eu^{2+} σ_{abs} is calculated according to $\sigma_{abs} = \alpha/N$. Here the absorption coefficient α is assumed to be 100 cm^{-1} and the density of Eu^{2+} N is on the order of 10^{20} cm^{-3} , which corresponds to $\sim 1 \text{ mol}\%$ Eu^{2+} in a cubic unit cell with cell parameter $a = 0.6 \text{ nm}$ and $Z = 2$. The cross-section for optically stimulated detrapping σ_{osl} is several times larger than σ_{abs} , according to the results in $\text{SrAl}_2\text{O}_4:\text{Eu}^{2+}$ phosphor [10].

The recombination frequency ν_r has been reported to be in the range of 10^8 - 10^{12} Hz [37], and we take $\nu_r = \nu_t = 10^{10} \text{ Hz}$. The trapping coefficient A_t is estimated to be 10% of the phonon energy, which can be estimated from Raman scattering. For phonons with energy around 350 cm^{-1} , the frequency is 10^{13} Hz , leading to $A_t = 10^{12} \text{ Hz}$.

The irradiance due to the excitation light was estimated from the power of LED (several mW) and the surface area of the irradiated phosphor in TL measurements. It is easy to achieve a photon flux of 10^{15} - 10^{16} Hz/cm^2 .

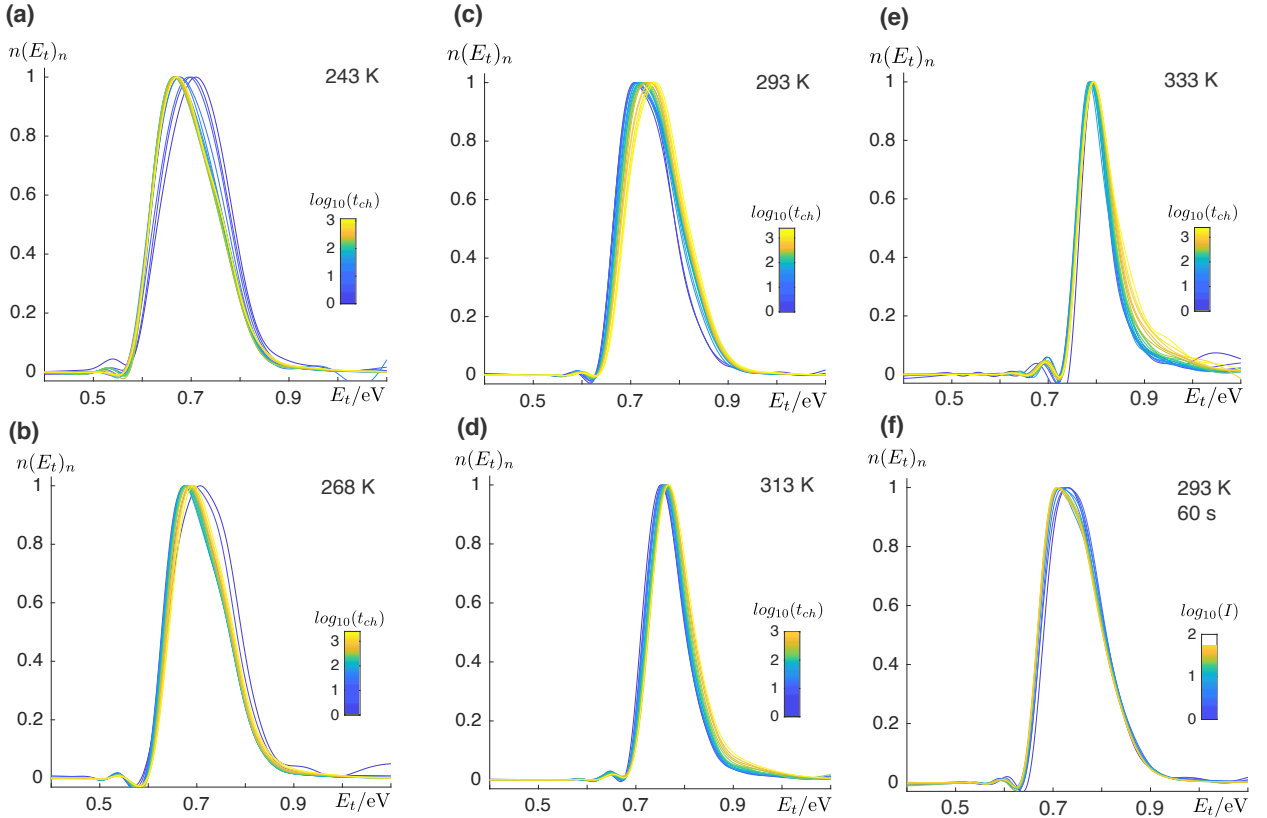


FIG. S5. **Normalized electron population function.** The normalized electron population function $n(E_t)_n$ at a fixed charging temperature T reaches to the steady-state profile with increasing charging time t_{ch} (from 2-2400 s). T was set to 243 (a), 268 (b), 293 (c), 313 (d) and 333 K (e), and the current of LED was 50 mA. (f) The $n(E_t)_n$ of fixed T and t_{ch} does not vary with increasing current of LED (1-50 mA).

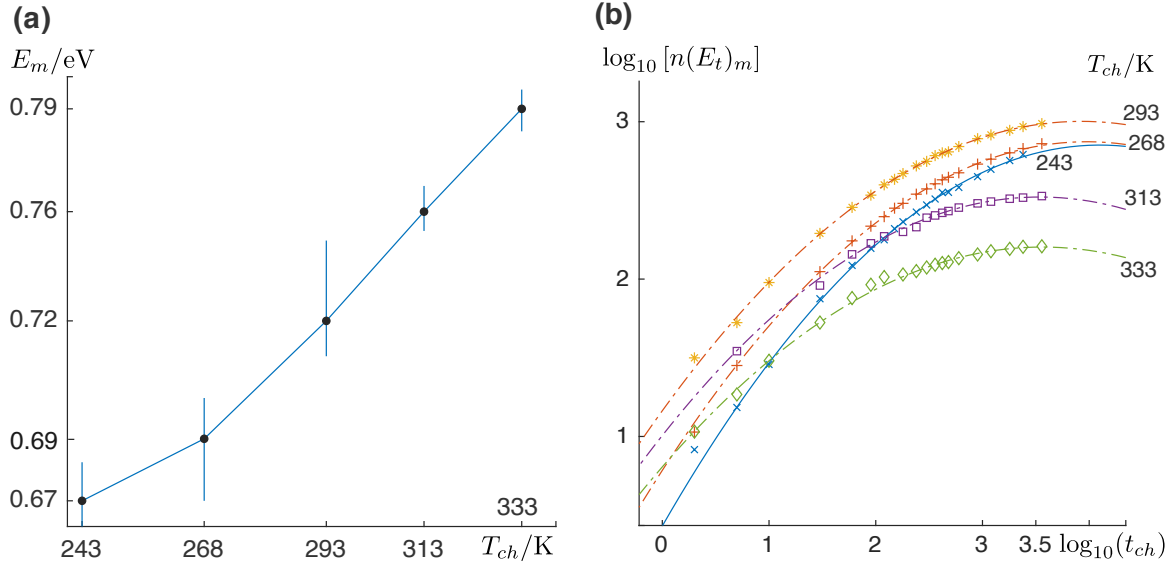


FIG. S6. **Dose dependency.** (a) The E_m is linear to T_{ch} . (b) The $\log_{10}[n(E_t)_m]$ is a quadratic function of $\log_{10}(t_{ch})$ for $T_{ch} = 243, 268, 293, 313,$ and 333 K.

IV. DOSE DEPENDENCY

The normalized electron population function,

$$n(E_t)_n = \frac{n(E_t)}{\max(n(E_t))}$$

reaches to the stable profile with increasing charging time t_{ch} from 2-2400 s, with charging temperature T_{ch} being 243, 268, 293, 313, and 333 K (Fig. S5a-e). Furthermore, the shape of $n(E_t)_n$ also stays unchanged with increasing LED current (1-50 mA), with a fixed charging duration $t_{ch} = 30$ s (Fig. S5f). The trap depth corresponding to the maximum of $n(E_t)_n$, i.e., E_m , is found linear to T_{ch} (Fig. S6a). It is noteworthy that E_m is just $\sim 3 k_B T_{ch}$ around the characteristic trap depth E_o . The maximum of $n(E_t)$, i.e., $n(E_t)_m$ is related to t_{ch} in such a way that $\log_{10}[n(E_t)_m]$ is a quadratic function of $\log_{10}(t_{ch})$ (Fig. S6b). To understand these behavior, the filling function $f(E_t, t_{ch})$ was simulated for t_{ch} ranging from 10^{-3} to 10^5 s (Fig. S7). $f(E_t, t_{ch})$ is a stage-like surface on the plane of $\log_{10}(t_{ch}) \times E_t$ (Fig. S7a). The edge of the surface can be inferred from the average curvature,

$$H = -\frac{1}{2} \nabla \cdot \vec{n}, \quad (\text{S12})$$

where \vec{n} is the normal of the surface. The extracted edges for several T_{ch} were shown in Fig. S7b. For each T_{ch} , there exists a turning point (E', t'_{ch}) such that $f(E_t, t_{ch})$ changes only slightly when $E_t > E'$ and $t_{ch} > t'_{ch}$. E' is linear with T_{ch} (also $\log_{10}(t_{ch})$), which explains the observation in Fig. S6a.

V. THE EFFECTIVE TRAP DEPTH

In this section, we give details of the filling function of TL curves with different charging temperature T_{ch} . After charging at T_{ch} for a duration of t_{ch} , the phosphor was cooled to $T_0 \leq T_{ch} - 30$ K at a rate of 0.5 K/s, reaching the initial condition of TL. The simulation parameters are $I_e = 5 \times 10^{15}$ Hz/cm², $t_{ch} = 10^2$ s, $\Delta E = 0.255$ eV, $\sigma_{abs} = 3 \times 10^{-18}$ cm², $\sigma_{osl} = 10^{-17}$ cm², $v_r = v_t = 10^{10}$ Hz, $k_{rad} = 1.58$ MHz and $A_t = 10^{12}$ Hz. The charging temperature T_{ch} is from 200 to 450K with a step of 25 K. The simulated filling function $f_{ch}(E_t, T_{ch})$ was normalized by its maximum $f_0(T_{ch})$,

$$\frac{f_{ch}(E_t, T_{ch})}{f_0(T_{ch})} = \exp \left[-\frac{E_t - E_o}{k_B(T_{ch} + \Delta T_{ch})} \right], \quad (\text{S13})$$

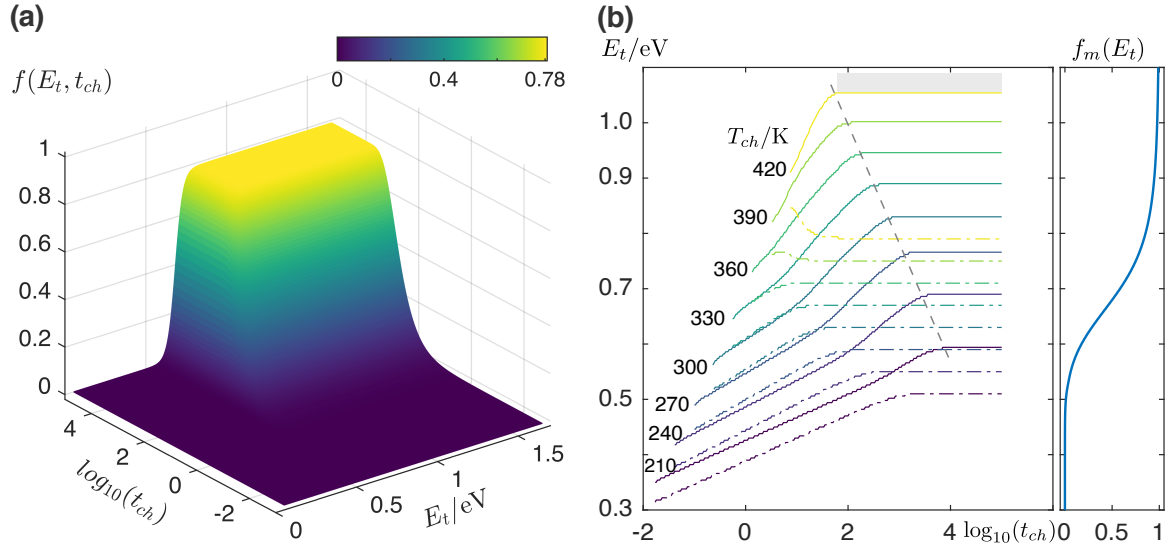


FIG. S7. **Simulation of $f(E_t, t_{ch})$.** (a) $f(E_t, t_{ch})$ at $T_{ch} = 300$ K shows a stage-like surface. (b) The edges of $f(E_t, t_{ch})$ and the $f_m(T_{ch})$ indicates the onset of $f_m(T_{ch})$ (grey dash-dot line) is linear to E_t (or $\log_{10}(t_{ch})$).

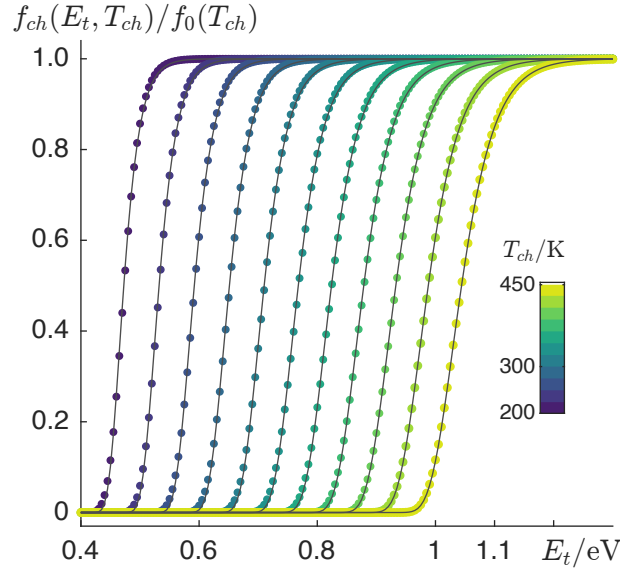


FIG. S8. **Filling functions at T_0 .** The normalized filling functions $f_{ch}(E_t, T_{ch})/f_0(T_{ch})$ at T_0 for T_{ch} from 200 to 450 K at a step of 25 K (dot). The solid lines are the fittings (Eqn. S13).

in which E_o is the effective trap depth and ΔT_{ch} a fitting parameter. The simulated filling function (Fig. S8, dots) can be fitted by the double exponential function Eqn. S13 (Fig. S8, solid line). The effective trap depth E_o and the associated ΔT_{ch} were tabulated in Table S1.

VI. EVALUATING THE EFFECTS OF GLOBAL RETRAPPING

We consider the effect of retrapping among traps here. The filling function moves toward deep traps accordingly with the effective trap depth

$$E_o = k_B T_{ch} \ln(v_r t_0) \quad (\text{S14})$$

TABLE S1. The effective trap depth E_o and the ΔT_{ch} at T_0 for different T_{ch} .

T_{ch}/K	$\Delta T_{ch}/\text{K}$	E_o/eV
200	19.4	0.466
225	20.2	0.525
250	21.0	0.583
275	22.0	0.642
300	23.0	0.700
325	24.2	0.757
350	23.6	0.812
375	18.8	0.866
400	10.8	0.920
425	2.9	0.974
450	-2.3	1.030

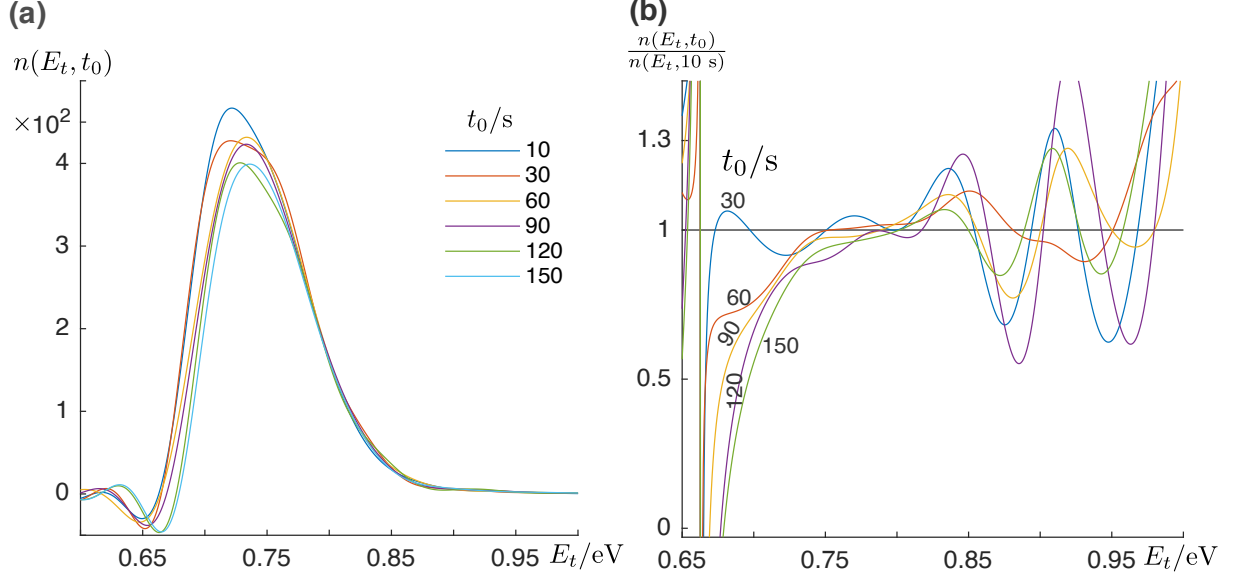


FIG. S9. **Delay time.** (a) The electron population function $n(E_t, t_0)$ is a function of delay time t_0 . (b) The magnitude of $\frac{n(E_t, t_0)}{n(E_t, 10 \text{ s})}$ does not show systematic increase with increasing delay time t_0 .

at a delay time t_0 . Electrons trapped around E_o can jump either to shallow traps ($E_t < E_o$) which is almost empty or to deep trap ($E_t > E_o$) which is effectively filled to up to $f_0(T_{ch})$. As electrons in shallow traps detrapp faster than those in deep traps, an increase in magnitude of filling $f_0(T_{ch})$ of deep traps increases with increasing delay time t_0 . Fig. S9 shows that there is not significant increase of $f_0(T_{ch}, t_0)$ relative to $f_0(T_{ch}, 10 \text{ s})$. The oscillations are due to uncertainties of regularization method. This suggests that retrapping among traps is not important for such a heating profile. However, this effect is important when the density of electrons at the excited states of traps is increased significantly by optical stimulation [49] or stress stimulation [28], leading to a re-distribution of electrons among traps.